

# Journal of Geotechnical and Geoenvironmental Engineering

## Modeling the Stress-Dilatancy Relationship of Unsaturated Silica Sand in Triaxial Compression Tests

--Manuscript Draft--

<b>Manuscript Number:</b>	GTENG-5233R2	
<b>Full Title:</b>	Modeling the Stress-Dilatancy Relationship of Unsaturated Silica Sand in Triaxial Compression Tests	
<b>Manuscript Region of Origin:</b>	UNITED KINGDOM	
<b>Article Type:</b>	Technical Paper	
<b>Funding Information:</b>	Schweizerischer Nationalfonds zur Förderung der Wissenschaftlichen Forschung (CH) (P1SKP2 158621)	Mr Elliot James Fern
	Seventh Framework Programme (BE) (PIAP-GA-2012-324522)	Not applicable
<b>Abstract:</b>	<p>It is well known that partial saturation increases the shear strength and dilatancy of unsaturated sand. However, little research has been carried out on the actual stress-dilatancy relationship. This paper shows that the increase in peak shear strength caused by partial saturation is consistent with an increase in dilatancy and that conventional stress-dilatancy theories are still valid for unsaturated sand. The use of state indexes as a proxy for dilatancy were investigated and extended to unsaturated sands. Additionally, these indexes can be used to establish a critical state line based on material properties only. The validity of the stress-dilatancy theories and the use of state indexes offer simplicity in modeling the shear behavior of unsaturated sand. This will be demonstrated in this paper with the Nor-Sand model, and with which the wetting collapse can be explained as a consequence of a loss of dilatancy characteristics.</p>	
<b>Corresponding Author:</b>	Elliot James Fern, MSc University of Cambridge Cambridge, UNITED KINGDOM	
<b>Corresponding Author E-Mail:</b>	jf497@cam.ac.uk;james.fern@bluewin.ch	
<b>Order of Authors:</b>	Elliot James Fern, MSc	
	Dilan Jeyachandran Robert, PhD	
	Kenichi Soga, PhD	
<b>Additional Information:</b>		
<b>Question</b>	<b>Response</b>	
Is the article being considered for more than one journal? The Journal of Geotechnical and Geoenvironmental Engineering does not review manuscripts that are being submitted simultaneously to another organization or ASCE journal for publication.	No	
Is this article already published? Material that has been previously published cannot be considered for publication by ASCE. A manuscript that has been published in a conference proceedings may be reviewed for publication only if it has been significantly revised. If you answer YES, please provide further explanation in your cover	No	

letter.	
<p>Have all the authors contributed to the study and approved the final version? All authors must have contributed to the study, seen the final draft of the manuscript, and accept responsibility for its contents. It is unethical to list someone as a coauthor who does not want to be associated with the study and who has never seen the manuscript.</p>	Yes
<p>Was an earlier version of the paper previously considered and declined by ASCE? Declined manuscripts are sent through the review process again. If your manuscript has been submitted to us before under a different title, please provide that title in the space provided below. It is our policy to inform an editor that a manuscript has been previously reviewed, even when it has been reviewed by a different Division, Institute, or Council within ASCE.</p>	No
<p>Do your table titles/figure captions cite other sources? If you used a figure/table from another source, written permission for print and online use must be attached in PDF format. Permission letters must state that permission is granted in both forms of media. If you used data from another source to create your own figure/table, the data is adapted and therefore obtaining permission is not required.</p>	No
<p>Does your paper exceed 10,000 words? If YES, please provide justification in your cover letter. If you need help estimating word length, see our sizing worksheet at this link: <a href="#">Sizing Worksheet</a>. If you have questions about the Sizing Worksheet, please see the <a href="#">Sizing Worksheet Instructions</a>.</p>	No
<p>Estimates for color figures in the printed journal begin at \$924. Cost increases depend on the number and size of figures. Do you intend for any figure to be printed in color? If YES, how many and which ones? Please provide a total count and also list them by figure number.</p>	No
<p>Is this manuscript a companion to one already submitted/or being submitted? If yes, please note whether this is part I, II, or III. Please make sure all related papers are uploaded on the same day and provide the date of submission, title, and authors of each.</p>	No

Is this manuscript part of a Special Issue? If yes, please provide the Special Issue title and name of the guest editor.	No
Did you include your ASCE Membership credentials in your author byline?	No
To read ASCE's Data Sharing Policy, please click on the "Instructions" link associated with this question. According to this policy, you are required to report on any materials sharing restrictions in your cover letter. Are you restricted from sharing your data & materials? If yes, did you report on these in your cover letter?	No

# Modeling the Stress-Dilatancy Relationship of Unsaturated Silica Sand in Triaxial Compression Tests

Elliot James Fern<sup>1</sup>, Not a Member, ASCE

Dilan Jeyachandran Robert<sup>2</sup>, Not a Member, ASCE

Kenichi Soga<sup>1</sup>, Member, ASCE

## ABSTRACT

It is well known that partial saturation increases the shear strength and dilatancy of unsaturated sand. However, little research has been carried out on the actual stress-dilatancy relationship. This paper shows that the increase in peak shear strength caused by partial saturation is consistent with an increase in dilatancy, and that conventional stress-dilatancy theories are still valid for unsaturated sand. The use of state indexes, as a proxy for dilatancy, were investigated and extended to unsaturated sands. Additionally, these indexes can be used to establish a critical state line which is based on material properties only. The validity of the stress-dilatancy theories and the use of state indexes offer simplicity in modeling the shear behavior of unsaturated sand. This will be demonstrated in this paper with the Nor-Sand model, and with which the wetting collapse can be explained as a consequence of a loss of dilatancy characteristics.

**Keywords:** Stress-dilatancy theory, critical state theory, state indexes, unsaturated sand, constitutive modeling.

## INTRODUCTION

Since the early work of Taylor (1948), it has been recognized that the development of the shear strength is a consequence of grains interlocking and the critical state strength, which was shown by Roscoe et al. (1958) to be uniquely defined. Roscoe and Schofield (1963) were driven by this idea and expressed Taylor's stress-dilatancy theory in terms of stress invariants. However, it was

---

<sup>1</sup>Dept. of Engrg., Univ. of Cambridge, Trumpington St., Cambridge CB2 1PZ, United Kingdom. E-mail: jf497@cam.ac.uk.

<sup>2</sup>Sch. of Civ. Env. and Chem. of Engrg., RMIT Univ., GPO Box 2476, Melbourne VIC 3001, Australia

22 later recognized that the contribution of dilatancy, or interlocking, was not as significant as was  
 23 previously believed (*i.e.* Bolton 1986; Stroud 1971). Amongst others, Nova (1982) introduced a  
 24 dilatancy parameter to minimize the influence of dilatancy on the shear strength (Eq. 1).

$$\eta' = M + (N - 1)D \quad (1)$$

25 where  $\eta' = q/p'$  is the effective stress ratio with  $q$  the deviatoric stress and  $p'$  the mean effective  
 26 stress,  $M$  the critical state stress ratio,  $N$  the dilatancy parameter and  $D = \frac{d\varepsilon_v^p}{d\varepsilon_d^p}$  the dilatancy rate,  
 27  $d\varepsilon_v^p$  and  $d\varepsilon_d^p$ , respectively, the plastic volumetric and deviatoric strain increments.

28 Roscoe and Schofield (1963) established the Original Cam-Clay model from the stress-dilatancy  
 29 theory by assuming that the development of plastic volumetric strains followed the development  
 30 of the shear strength. In turn, Roscoe and Burland (1968) simplified the equation to formulate  
 31 the Modified Cam-Clay model. Roscoe (1970) later recognized the limitations of these models  
 32 in predicting the behavior of sand, and the necessity of introducing a hardening law based on a  
 33 strain invariant which would relate to the critical state. Jefferies (1993) suggested using the state  
 34 parameter (Been and Jefferies 1985) as a strain invariant (Eq. 2).

$$\psi = e - e_{cs} \quad (2)$$

35 where  $\psi$  is the state parameter,  $e$  the void ratio and  $e_{cs}$  the critical state void ratio.

36 The state parameter is a measurement of how much the sand has to contract or dilate in order  
 37 to reach the critical state. Jefferies (1993) then derived Nova's stress-dilatancy rule (Eq. 1) to  
 38 formulate the Nor-Sand model which, unlike the Cam-Clay models, included the void ratio as a  
 39 model variable. It also allowed plasticity to take place prior to the peak state.

40 The idea of introducing plasticity before the peak state was not new (Drucker et al. 1957).  
 41 Dafalias and Popov (1975) introduced it in a bounding surface model for cyclic loading, and Bardet  
 42 (1986) for triaxial loading. Hashiguchi and Chen (1998) introduced the sub-loading surface con-  
 43 cept, which also allowed plasticity to take place prior to the peak state by reformulating the con-

44 sistency condition. This allowed existing models, such as the Cam-Clay models, to be updated.  
45 Nor-Sand resembles these models in the sense that it predicts the hardening rate by comparing the  
46 current stress state with an estimated peak state.

47 Despite the fact that all Cambridge-type theories and models originate from the stress-dilatancy  
48 theory, it is surprising that little attention has been given to these relationships when modeling the  
49 behavior of partially saturated soils. Alonso et al. (1990) carried out a straightforward extension of  
50 the modified Cam-Clay model for unsaturated soils by introducing the loading-collapse (LC) curve.  
51 However, it did not include sub-loading surface and hence plasticity prior to the peak state. The  
52 LC curve enhanced the preconsolidation pressure with partial saturation. Therefore, it assumed  
53 that the peak strength was a yielding point which violates the stress dilatancy theory. Cui and De-  
54 lage (1996) also observed the enhancement by partial saturation of both the peak strength and the  
55 dilatancy rates. However, they still considered the peak state as a yielding point and, consequently,  
56 suggested a different shape of the yield surface to accommodate this modeling assumption. Chiu  
57 and Ng (2003) understood the importance of the stress-dilatancy theory in developing new stress-  
58 strain relationships for unsaturated sand, and proposed a model which would capture the peak  
59 strength as a consequence of dilatancy. However, this model was developed on mildly dilative  
60 soils, which did not offer sufficient data to extend any state index (Ng and Menzies 2007). Rus-  
61 sell and Khalili (2006) suggested a bounding surface model for both unsaturated clays and sands,  
62 which allowed plasticity to take place prior to the peak and was able to predict wetting-collapses  
63 without introducing a loading-collapse curve. Many of the available models show good abilities  
64 in modeling the behavior of unsaturated soils (D'Onza et al. 2011). However, these models relied  
65 on a vast number of model parameters, which do not necessarily have any physical meaning or are  
66 not easily quantifiable.

67 This paper aims to demonstrate the validity of the stress-dilatancy theory for unsaturated sand,  
68 and explains the increase of peak strength as the consequence of an increase of the dilatancy rates.  
69 The use of state indexes as proxies for dilatancy can be extended to unsaturated sand, and can be  
70 used to predict the peak state. The ability to predict both the critical state and peak states offers

71 simplicity in modeling the behavior of unsaturated sands, and will be demonstrated with the Nor-  
 72 Sand model. It will also be shown that the on-set of a wetting collapse can be understood, and  
 73 modeled as a loss of dilatancy characteristics rather than a yielding point.

## 74 **CRITICAL STATE STRENGTH AND STRESS VARIABLES**

75 The critical state theory (Roscoe et al. 1958) suggests that any soils sheared sufficiently will  
 76 ultimately reach a unique state called the critical state. In this state, the soil will be continuously  
 77 deformed without any changes in volume or stress state. Therefore, the stress-dilatancy theory (Eq.  
 78 1) and the state parameter (Eq. 2) at critical state yield to Eq. 3.

$$D := 0 \quad \rightarrow \quad \eta' = M, \quad \psi = 0 \quad (3)$$

79 Partial saturation is known to enhance the critical state strength of soil. However, its expression  
 80 depends on the choice of the stress variables. There is little consensus on which variables to use.  
 81 Bishop (1959) suggested a generalized formulation of Terzaghi's effective stress (Eq. 4) which  
 82 directly took into account the contribution of partial saturation through suction  $s$  and a coupling  
 83 parameter  $\chi$ .

$$p' = p^{net} + \chi s \quad (4)$$

84 where  $p'$  is the mean effective stress,  $p^{net} = p^{tot} - p_a$  the mean net stress with  $p^{tot}$  the mean total  
 85 stress and  $p_a$  the pore air pressure,  $s = p_a - p_w$  the matric suction with  $p_w$  the pore water pressure  
 86 and  $\chi$  the coupling parameter.

87 Bishop's effective stress (Eq. 4) provides a stress variable, which explains any change in strains  
 88 by a change in stresses. However, the quantification of the coupling parameter  $\chi$  has been a matter  
 89 of debate since its original formulation (*i.e.* Aitchison 1960; Bishop and Blight 1963; Coleman  
 90 1962). Its incapacity to explain the wetting-collapse in the framework of elasticity made it unpopu-  
 91 lar (Jennings and Burland 1962), despite evidence that the wetting-collapse was a plastic behavior  
 92 (Leonards 1962). It was only later that the plastic nature of the wetting-collapse reached a consen-  
 93 sus with the introduction of the LC-curve (Alonso et al. 1990). However, the use of Bishop's effec-

94 tive stress was still unpopular, as it could not explain the peak strength in an elastic-plastic frame-  
95 work. In this context, it was acknowledge that the coupling parameter  $\chi$  would mainly depend on  
96 the degree saturation  $S_w$  (Bishop and Blight 1963) but would have to include some dependency  
97 to pressure (Aitchison 1960), to the stress history (Coleman 1962), and even to the soil structure  
98 (Alonso et al. 2010). Khalili et al. (2004) pointed out that most arguments against Bishop's effec-  
99 tive stress were formulated within the context of linear elasticity. Non-recoverable deformations,  
100 such as dilation or collapses, could not even be explained for saturated soils in terms of effective  
101 stresses alone without invoking appropriate plasticity theories. It is known for saturated sand that  
102 the peak strength is a consequence of dilatancy, and that plasticity takes place prior to the peak.  
103 Dilatancy is density and pressure dependent (Been and Jefferies 1985; Bolton 1986) and plasticity  
104 is stress path dependent. Therefore, it is believed that the only reason that the peak strength could  
105 not be predicted with Bishop's effective stress is due to limitations of the elastic-plastic modeling  
106 framework.

107 Khalili and Khabbaz (1998) suggested a non-linear coupling parameter  $\chi$  as a function of ma-  
108 tric suction  $s$  only, and overcame some of the historical skepticism in using Bishop's effective  
109 stress. The non-linearity was necessary as it was used to predict the peak strength in associa-  
110 tion with a Mohr-Coulomb model for unsaturated soils (Fredlund et al. 1978), which is set in the  
111 elastic-plastic framework. It can be argued that the proposed non-linear coupling parameter  $\chi$  en-  
112 capsulated the non-linearity present in the soil water retention curve (SWRC). However, it was  
113 later shown that this empirical relationship could be adapted to capture the critical state strength  
114 (Loret and Khalili 2000). However, the coupling parameter  $\chi$  was found to be different for unsat-  
115 urated clays and sands (Russell and Khalili 2006). Nuth (2009) reviewed the data of Wheeler and  
116 Sivakumar (1995), Maatouk et al. (1995), Cui and Delage (1996), Geiser (1999), Rampino et al.  
117 (2000) and Toll and Ong (2003), and showed that the critical state stress ratio  $M$  was uniquely  
118 defined when the coupling parameter  $\chi$  was taken as the degree of saturation. Other authors (*i.e.*  
119 Bolzon et al. 1996; Lu and Likos 2004) suggested using the effective degree of saturation (Eq. 5)  
120 as a coupling parameter  $\chi$ . Alonso et al. (2010) suggested a similar coupling parameter  $\chi$  which



121 yields to Eq. 5 for silica sand.

$$\chi = S'_w = \frac{S_w - S_{res}}{1 - S_{res}} \quad \text{if } S_w \geq S_{res} \quad (5)$$

122 where  $S'_w$  is the effective degree of saturation,  $S_w$  the degree of saturation and  $S_{res}$  the residual  
123 degree of saturation.

124 The advantage of using the effective degree of saturation  $S'_w$  instead of the degree of saturation  
125  $S_w$  is that it avoids exponentially increasing values of suction stress ( $s \cdot S'_w$ ) around the residual  
126 degree of saturation, whilst not affecting much the suction stress at higher degree of saturation.

## 127 **CHIBA SAND**

128 In this study, the mechanical behavior of an unsaturated silica sand, called Chiba, sand was  
129 undertaken. Chiba sand is a poorly graded silica sand with a particle size ranging from 0.01 mm  
130 to 1.00 mm. It has a coefficient of uniformity of 2.1 and a coefficient of curvature of 1.1. The  
131 grain-size distribution was obtained by sieving and sedimentation and is shown in Fig. 1(a). The  
132 minimum and maximum void ratios were found to be respectively 0.500 and 0.946, and its specific  
133 gravity 2.72. The critical state friction angle was found to be 33°, a typical value for silica sand.

134 The SWRC was obtained for the drying path by Robert (2010) and for three different densities  
135 using the axis translation technique. The specimens were subjected to matric suctions of 2 to 60  
136 kPa. Pressure ranging from 2 to 10 kPa were applied by means of negative water head (buret)  
137 and the 60 kPa with a pressure plate. Complimentary investigations were carried out on a loose  
138 specimen and the air entry value  $s_e$ , which was found to be 0.5 kPa, the residual degree of saturation  
139 around 20%, and a very small hysteresis was found. Similar results were obtained by Schnellmann  
140 et al. (2013) for Eschenbach Sand and Russell (2004) for Kurnell Sand. However, the SWRC were  
141 obtained using similar techniques which could explain similar results and high residual degree of  
142 saturation. The SWRC were fitted with a van Genuchten (1980) model (Eq. 6) for each density and  
143 the results are summarized in Table 1. Fig 1(b) shows the experimental results and model fittings.

$$S'_w = [1 + (\alpha_w s)^{n_w}]^{-m_w} \quad (6)$$

144 where  $a_w$ ,  $n_w$ ,  $m_w$  are model parameters.

145 A series of constant-water-content triaxial compression tests were carried out on Chiba sand  
 146 and additional information on the test program is given in Appendix A. The choice of using this  
 147 data set instead of suction-controlled tests was motivated by the wide range of initial densities  
 148 and pressures. Furthermore, the accuracy of a water or air controller is typically around 1 kPa,  
 149 which makes suction-controlled tests very difficult to carry out on unsaturated sand in the funicu-  
 150 lar regime. These tests were carried out in duplicates at two different strain rates, which allowed a  
 151 comparison of the volumetric deformation, and to detect any inconsistency in the measurements.  
 152 The constant-water-content test implies that the mass of water is conserved throughout the en-  
 153 tire test and, hence, the degree of saturation and the matric suction were free to change with the  
 154 volumetric deformation. Toll (1988) and Ng and Menzies (2007) showed that the changes in ma-  
 155 tric suction in granular material were consistent with the changes in volume for matric suction  
 156 within the funicular regime. Sand tends to dilate and the degree of saturations decreases through-  
 157 out most of the test. Therefore, it is reasonable to estimate the matric suction of dilative sands  
 158 with the drying SWRC. Russell and Khalili (2006) carried out both constant-water-content and  
 159 suction-controlled triaxial compression tests on Kurnell sand, and showed that both methods gave  
 160 similar results. Fern et al. (2015) also compared suction-controlled and constant-water-content tri-  
 161 axial compression tests of Chiba sand, and also showed that they gave similar results. The matric  
 162 suction of the constant-water-content tests was estimated with the SWRC. However, the matric  
 163 suction in sand is typically lower than 10 kPa and, hence, its contribution to the mean effective  
 164 stress is limited. Nevertheless, the validity of the effective stress principle is paramount for the  
 165 stress-dilatancy theory and hence for the analysis.

## 166 **STRESS-DILATANCY RELATIONSHIP**

167 The results of triaxial tests are commonly presented in two figures, one for the shear strength

168 and one for the volumetric behaviour. However, it is possible to present both behaviours in a single  
169 figure in the form of a stress-dilatancy curve. The use of a stress ratio allows a better comparison  
170 between tests at different confining pressures. Fig. 2 shows a schematic description of a triaxial  
171 compression test. Fig. 2(a) shows the development of the effective stress ratio with dilatancy, Fig.  
172 2(b) the development of strength with deviatoric strains and Fig. 2(c) the volume changes with  
173 deviatoric strains. In triaxial compression tests, the specimen first undergoes a short contraction  
174 of typically 1% volumetric strain for 1% to 5% deviatoric strain (points A to B). It can be seen  
175 that this contraction appears to be more significant in the stress-dilatancy curve due to the low  
176 stresses ( $\eta' = q/p'$ ). At point B, the specimen starts dilating and developing a peak strength which  
177 is reached at point C. The specimen then softens from point C to B' but is still dilating. It reaches  
178 the critical state at point B'.

179 In order to facilitate the reading, all the figures shown in this paper have the same marker  
180 and color convention. The markers correspond to the three different initial densities ( $\circ$  loose,  
181  $\square$  medium-dense and  $\diamond$  dense) and the color to their initial water content - black for saturated  
182 specimens, and shadings of gray for partially saturated specimens. The void ratio and the degree  
183 of saturation used for the analyses were updated throughout the tests with the volumetric strain.

184 Fig. 3 shows the stress-dilatancy curves of the constant-water-content tests with an axial rate  
185 of 0.1%/min. The three top sub-figures (a-c) show the results for the dense specimens, the three  
186 middle sub-figures (d-f) for the medium-dense and the three bottom sub-figures (g-i) for the loose  
187 specimens. Each series of sub-figures (a-c, d-f & g-i) are, respectively, for three different initial  
188 mean net pressures ( $p_0^{net} = 20, 40 \text{ \& } 80 \text{ kPa}$ ). Each sub-figure contains two stress-dilatancy curves,  
189 respectively, for a water content of 10% and 17%. A trend line has been plotted for each test in  
190 order to facilitate the interpretation of results.

191 The results show an initial contraction ( $D > 0$ ) followed by dilation ( $D < 0$ ). The magnitude  
192 of the contraction and dilation phases increased as the initial density increased. The transition  
193 point between both phases ( $D = 0$ ) occurred at a stress state which, in some cases, differed from  
194 the critical state. The loose and medium-dense specimens (d-i) reached this transition state at

195 an effective stress ratio lower or equal to the critical state value and the dense specimens (a-c)  
196 for values equal or slightly higher. It is also common for saturated sand to exhibit a transition  
197 point different from the critical state value (Jefferies and Been 2006; Jefferies and Shuttle 2011).  
198 Beyond this point, all specimens dilated. The minimum dilatancy rate was reached in the region of  
199 the maximum effective stress ratio. The results show that there was an increase in the peak strength  
200 and the dilatancy rates with density, but also with partial saturation. Fig. 4(a) shows the peak states  
201  $(D_{min}, \eta'_{max})$  of all tests in which the influence of partial saturation can clearly be seen. The peak  
202 strengths and dilatancy rates evolved simultaneously with density and partial saturation following  
203 the same stress-dilatancy slope. This slope defines the dilatancy parameter  $N$  in Nova's flow rule  
204 (Eq. 1) and was found to be 0.3. Fig. 4(b) shows a schematic description of the observed increases  
205 in peak states. The influence of partial saturation on the peak state was more significant for dense  
206 specimens than for the loose ones. Specimens softened after reaching the peaks state and headed  
207 towards the critical state. The critical state stress ratio ( $\eta'_{cs} = M$ ) was uniquely defined when  
208 expressed as effective stresses. However, the contribution of suction on the critical state effective  
209 stresses is small, albeit necessary from a theoretical point of view. The results show that, despite  
210 tending towards the critical state, dense specimens underwent strain localization. This can be seen  
211 in Fig. 3(a-c). The stress-dilatancy curve suddenly goes from a smooth softening slope to a plateau  
212 ( $\eta' = cst > M, D \rightarrow 0$ ). The strain localization in dense specimens prevents them from reaching  
213 the critical state. This issue has been discussed for saturated sand in Roscoe (1970) and Desrues  
214 et al. (1996). Higo et al. (2011) showed that partial saturation increased the susceptibility of dense  
215 specimens to exhibit strain localization. Loose specimens were not sheared sufficiently to reach  
216 the critical state, and the final stress state did not reach the nil dilatancy condition.

217 Despite little research on the behavior of unsaturated sands, there is some experimental evi-  
218 dence of the enhancement of both the peak strength and the dilatancy rates. However, the investi-  
219 gation of the dilatancy characteristics requires a large number of tests in order to capture the con-  
220 tribution of density, pressure and partial saturation, which are rarely available. Schnellmann et al.  
221 (2013) carried out suction-controlled direct shear tests on a silica sand called Eschenbach sand,

222 and the results clearly show an enhancement of the peak strength and dilatancy rates with little  
223 changes in the critical state strength. However, the testing program was limited to a single density.  
224 Russell (2004) carried out triaxial compression tests on unsaturated Kurnell sand at two different  
225 densities but at two different pressures. Additionally, the specimens were largely in the pendular  
226 regime. Robert (2010) carried out constant-water-content direct shear tests and suction-controlled  
227 triaxial compression tests on Chiba sand and Cornell sand. The direct shear tests clearly showed an  
228 enhancement of the dilatancy characteristics with partial saturation. The suction-controlled tests  
229 were carried out for one density which limited the investigation of the dilatancy characteristics.

230 Toll (1988, 1990) suggested that partial saturation caused a modification of the soil fabric  
231 which disturbed the way the packets of grains override one another during the development of  
232 strength. Ng and Menzies (2007) also believed in a modification of the soil fabric by partial sat-  
233 uration. Scholtès et al. (2009) concluded, on the basis of discrete element modeling, that partial  
234 saturation would inevitably result in a different fabric as the formation of new inter-particles bonds  
235 would modify the way force are transmitted from one end of the specimen to another. Oda (1972),  
236 Tatsuoka (1987) and Lam and Tatsuoka (1988) showed for saturated Toyoura sand that a modifi-  
237 cation of the soil fabric caused an enhancement of the peak strength and the minimum dilatancy  
238 rate. Furthermore, Oda (1972) observed that the stress-dilatancy slope, captured by the dilatancy  
239 parameter  $N$  in Eq. 1, remained constant. The results suggest that the enhancement of the mini-  
240 mum dilatancy rate is due to a modification of the soil fabric caused by the presence of menisci.  
241 From a micro-mechanical point of view, the formation of menisci results in the enhancement of  
242 tensile strength and, from a macro-mechanical point of view, the formation of menisci results in an  
243 enhancement of the dilatancy characteristics and effective stresses, and therefore of strength. The  
244 effective stress alone is insufficient to explain the enhancement of the peak strength.

## 245 **STATE INDEXES**

246 The prediction of the minimum dilatancy rate can be achieved with state indexes such as the  
247 state parameter (Been and Jefferies 1985) or the relative dilatancy index (Bolton 1986). They have  
248 been shown to be powerful modeling proxies for dilatancy and are commonly used in constitutive

249 modeling. The state parameter (Eq. 2) is a theoretical state index which was developed from the  
 250 critical state theory and relies on it to be quantified. Jefferies (1993) suggested estimating the  
 251 minimum dilatancy rate by converting the state parameter with the dilatancy coefficient  $X$  (Eq. 7)  
 252 introduced by Jefferies and Shuttle (2002). It was later recognized by (Jefferies and Been 2006)  
 253 that the dilatancy coefficient  $X$  would be fabric dependent.

$$D_{min} = X \cdot \psi \quad (7)$$

254 where  $\psi$  is the state parameter,  $e$  the void ratio and  $e_{cs}$  the critical state void ratio

255 An alternative to the state parameter is the relative dilatancy index (Eq. 8) which is a better  
 256 suited index for experimental data as it does not require the establishment of the critical state line.

$$I_R = I_D \cdot I_C - 1 \quad (8)$$

257 The relative dilatancy index takes into account the contributions of density through the relative  
 258 density index (Eq. 9), and pressure through the relative pressure index (Eq. 10).

$$I_D = \frac{e_{max} - e}{e_{max} - e_{min}} \quad (9)$$

$$I_C = \ln(Q/p') \quad (10)$$

260 Bolton (1986) suggested using the relative dilatancy index as a proxy for the maximum axial  
 261 dilatancy rate  $D_{1,min}$  by using a dilatancy coefficient  $\alpha$ . Tatsuoka (1987) pointed out that this  
 262 conversion was fabric dependent. The maximum axial dilatancy rate  $D_{1,min}$  is fully equivalent to  
 263 the dilatancy rate  $D$  defined in this paper. However, the conversion from the axial dilatancy rate  
 264 to a dilatancy rate is non-linear. The same applies to the relative dilatancy index and the state  
 265 parameter despite both indexes being fully equivalent.

$$D_{1,max} = max \left( \frac{d\varepsilon_v}{d\varepsilon_1} \right) = \alpha \cdot I_R \quad (11)$$

266 where  $I_R$  is the relative dilatancy index,  $I_D$  the relative density index,  $I_C$  the relative pressure  
267 index,  $e_{max}$ ,  $e_{min}$  and  $e$  are respectively the maximum, minimum and actual void ratios and  $Q$  the  
268 crushing pressure for which values are given in Bolton (1986).

269 The relative dilatancy index is believed to be valid for unsaturated sand as its components  
270 remain valid. The relative density index is a description of the pore space regardless of the fluids  
271 inside and, therefore, should be independent of partial saturation. Both the minimum and the  
272 maximum void ratio are considered to be material properties. The crushing pressure is a property  
273 of the mineral as discussed in (Bolton 1986). If the effective stress principle is valid for unsaturated  
274 sand, the relative dilatancy index should also be valid. However, an increase in effective stresses  
275 by partial saturation would result in a lower relative dilatancy index and in dilatancy rate for a  
276 given  $\alpha$ . An increase in the inter-particle bonding forces, due to the presence of menisci, would  
277 prevent some dilatancy as particles are bonded to one another and, hence, the relative dilatancy  
278 index is correctly smaller. However, experimental observations (Fig. 4a) show an enhancement of  
279 the dilatancy rates which suggests that  $\alpha$  would change with partial saturation.

280 There is an alternative approach to investigate the validity of the relative dilatancy index.  
281 Mitchell and Soga (2005) showed that the relative dilatancy index could be converted into a critical  
282 state line as the relative dilatancy index are nil at critical state (Eq. 12) and that the critical state  
283 density is not influenced by the soil fabric.

$$e_{cs} = e_{max} - \frac{e_{max} - e_{min}}{\ln(Q/p')} \quad (12)$$

284 This critical state line is non-linear with a sharp change in slope as the pressure increases  
285 towards the crushing pressure. Fig. 5(a) shows the critical state line for saturated Toyoura sand  
286 from Verdugo and Ishihara (1996). It demonstrates that the relative dilatancy index can predict  
287 the critical state void ratio of saturated silica sand. Russell and Khalili (2006) noticed that, unlike  
288 for unsaturated clays, the critical state line of Kurnell sand was the same as for saturated and  
289 unsaturated sands when stresses were expressed as effective (Fig. 5b).

290 Fig. 6(a) and (b) show the evolution of void ratio for dry and unsaturated medium-dense Chiba  
291 sand, respectively, for an axial strain rate of 0.1%/min and 5.0%/min. The choice of presenting  
292 the medium-dense tests was to avoid tests which were not sufficiently sheared or had undergone  
293 strain localization. The dry specimens were prepared by dry pluviation and the unsaturated by wet  
294 tamping which inferred different fabrics to the soil. However, both the dry and the unsaturated  
295 specimens reached the same critical state line. The results suggest that the critical state line is  
296 unique for unsaturated Chiba sand and that the relative dilatancy index is valid. The establishment  
297 of a critical state for unsaturated sand permits a quantification of the state parameter. This is a  
298 major difference with other researchers who used conventional critical state lines to quantify the  
299 state parameter.

300 Fig. 7(a) and (b) show, respectively, the relative dilatancy index and the state parameter for  
301 Chiba sand for the different strain rates which offered redundancy in the computed variables.  
302 Whilst the relative dilatancy index and the state parameter are still valid for unsaturated sand,  
303 the results suggest that their conversion to a dilatancy rate are partial saturation dependent. This is  
304 consistent with Tatsuoka (1987) and Jefferies and Been (2006) who suggested a dependency to the  
305 soil fabric.

306 It is common in unsaturated soil mechanics, but not exclusive, to use the matric suction as a  
307 model variable. Sands have a very small air entry value, often below 1 kPa (*i.e.* Likos et al. 2010).  
308 Therefore, the error committed by neglecting this air entry value is limited. It is then possible to  
309 use the degree of saturation  $S_w$  as a model variable which allows the model to be formulated over  
310 the entire domain of saturation. There is some evidence that the shear strength and dilatancy drops  
311 beyond the residual degree of saturation (*i.e.* Donald 1956; Vanapalli et al. 1996; Lu and Likos  
312 2006). Robert (2010) showed this drop in strength for Chiba sand in direct shear tests. Russell and  
313 Khalili (2006) showed evidence of loss of strength with increasing suction in suction-controlled  
314 oedometer which is consistent with the collapse of a sand castle by drying. By using the degree of  
315 saturation as a model variable, it is possible to differentiate the changes in mechanical properties  
316 by drying and wetting.



317 The enhancement of the dilatancy coefficient with partial saturation can be decomposed into a  
 318 saturated term and a partially saturated term (Eq. 13).

$$X = X_{sat} + \Delta X \cdot f_{(S'_w)} \quad (13)$$

319 where  $X_{sat}$  is the dilatancy coefficient for saturated and dry conditions,  $\Delta X$  the maximum en-  
 320 hancement value and  $f_{(S'_w)}$  the shape function. The enhanced part of the dilatancy coefficient can  
 321 be formulated as a maximum enhancement  $\Delta X$ , which would occur at a certain degree of satura-  
 322 tion  $S_w^{max}$ , and a shape function.

323 Vanapalli et al. (1996) suggested that the maximum strength enhancement would occur around  
 324 the residual degree of saturation. Therefore, the degree of saturation at maximum strength would  
 325 relate to the residual degree of saturation. However, in order to be general and avoid confusion,  
 326 the degree of saturation at maximum enhancement will be referred to as  $S_w^{max}$ . The shape function  
 327 can be formulated as a function of the effective degree of saturation  $S'_w$  and expressed in Eq. 14.

$$f_{(S'_w)} = \frac{\exp(-\beta \cdot S_w'^2) - \exp(-\beta)}{1 - \exp(-\beta)} \quad (14)$$

328 The effective degree of saturation, has a maximum value of 1 at  $S'_w = 0$  and 0 at  $S'_w = 1$ , can  
 329 be formulated over the entire domain of saturation as shown in Eq. 15.

$$S'_w = \begin{cases} \frac{S_w - S_w^{max}}{1 - S_w^{max}} & \text{if } S_w \geq S_w^{max} \\ \frac{S_w^{max} - S_w}{S_w^{max}} & \text{if } S_w < S_w^{max} \end{cases} \quad (15)$$

330 where  $f$  is the shape function,  $S'_w$  the effective degree of saturation,  $S_w^{max}$  the degree of saturation  
 331 at maximum enhancement and  $\beta$  the shape function coefficient.

332 Fig. 8(a) shows the shape function for different vales of  $\beta$  in which it can be seen that high  
 333 values of the shape parameter concentrate the enhancement around the nil effective degree of sat-

334 uration. The shape function is continuously derivable over the entire domain of saturation and for  
 335 any value of  $\beta$ . This implies that the value of  $\beta$  can differ from the wet and dry side. High values  
 336 of  $\beta$  minimizes the influence of the neglected air entry value at full saturation. Fig. 8(b) shows  
 337 the calibration of the shape function for the constant-water-content tests on Chiba sand. The black  
 338 markers are the mean values obtained from Fig. 7.

## 339 CONSTITUTIVE MODELING

340 The stress-dilatancy rule (Eq. 1) was shown to be valid for both saturated and partially satu-  
 341 rated sands which implies that existing constitutive models for saturated sands can be extended to  
 342 partially saturated conditions. The ability to predict the critical state effective stress ratio  $M$  and  
 343 the dilatancy rates at peak state offers unprecedented convenience in modeling. Jefferies (1993)  
 344 suggested a model called Nor-Sand which was developed from Nova's stress-dilatancy rule (Eq.  
 345 1) by means of normality (Drucker et al. 1957) and, therefore, preserves the shape of the yield  
 346 function for partially saturated conditions. The Nor-Sand models was made non-associative by  
 347 Borja and Andrade (2006) and will be used to demonstrate the enhancement by partial saturation  
 348 of the dilatancy characteristics.

349 The Nor-Sand model can be viewed as an Original Cam-Clay model (Roscoe and Schofield  
 350 1963) with sub-loading surface (Hashiguchi and Chen 1998) for sands and for which the maximum  
 351 yield surface is determined as a function of the dilatancy characteristics. It assumes that plasticity  
 352 takes place prior to the peak state. The Nor-Sand model sizes the yield and the potential surfaces  
 353 with the image pressures which correspond to the pressure at the tip of the surface as shown in Fig.  
 354 9. The image pressures are equal to the mean effective stress at critical state ( $p' = p_i = p_{i,p}$ ). Eqs.  
 355 16 and 17 give the yield and potential functions, respectively.

$$F = \eta' - \frac{M}{N_f} \left[ 1 + (N_f - 1) \left( \frac{p'}{p_i} \right)^{\frac{N}{1-N_f}} \right] \quad \text{for } N_f > N_p > 0 \quad (16)$$

$$P = \eta' - \frac{M}{N_p} \left[ 1 + (N_p - 1) \left( \frac{p'}{p_{i,p}} \right)^{\frac{N_p}{1-N_p}} \right] \quad \text{for } N_f > N_p > 0 \quad (17)$$

357 where  $F$  is the yield function,  $P$  the potential function,  $N_f$  and  $N_p$  the dilatancy parameters for  
 358 ,respectively, the yield and potential functions, and  $p_i$  and  $p_{i,p}$  the image pressures for the yield and  
 359 potential functions, respectively.

360 The inclusion of a new variable to capture the partial saturation implies that the consistency  
 361 condition has to be extended (Eq. 18) and the derivatives of the yield and potential functions have  
 362 to be obtained consequently.

$$dF = \frac{\partial F}{\partial \sigma} d\sigma + \frac{\partial F}{\partial p_i} \frac{\partial p_i}{\partial \varepsilon_d^p} d\varepsilon_d^p + \frac{\partial F}{\partial p_i} \frac{\partial p_i}{\partial S_w} dS_w \quad (18)$$

363 The Nor-Sand model assumes that the hardening and softening rates are proportional to the  
 364 distance between the current state, characterized by the image pressure  $p_i$ , and the maximum pre-  
 365 dicted state, characterized by the maximum image pressure  $p_{i,max}$ . The proportionality between  
 366 the hardening rate and the difference in image pressures defines the hardening modulus  $H$ . The  
 367 maximum image pressure is estimated by considering the dilatancy characteristics of the soil (Eq.  
 368 19).

$$\frac{p_{i,max}}{p'} = \left( 1 + D_{min} \cdot \frac{N_f}{M} \right)^{\frac{N_f-1}{N_f}} \quad (19)$$

370 where  $p_{i,max}$  is the maximum image pressure

371 The hardening concept is similar to the one expressed for bounding surface models (*i.e.* Russell  
 372 and Khalili 2006) or subloading surfaces (*e.g.* Hashiguchi and Chen 1998). The hardening rule  
 373 can be expressed as shown in Eq. 20.

$$\frac{\dot{p}_i}{\dot{\varepsilon}_d^p} = H \cdot M \exp \left( 1 - \frac{\eta'}{M} \right) \cdot (p_{i,max} - p_i) \quad (20)$$

374 where  $H = H_{min} \exp(\delta_H I_D)$  is the hardening modulus, which is dependent on the state parameter  
 375 (Jefferies and Been 2006), and  $H_{min}$  is the minimum hardening modulus for very loose sand and  
 376  $\delta_H$  its enhancement by density.

377 The prediction of minimum dilatancy rate (Eq. 21) was updated due to the non-associativity

378 (Borja and Andrade 2006) and for which the dilatancy parameter  $N_p$  is obtained from the stress-  
 379 dilatancy curves (Fig. 4).

$$D_{min} = \chi \cdot \frac{1 - N_p}{1 - N_f} \cdot \psi_i \quad (21)$$

380 Partial saturation enhances the mean effective stress and the dilatancy characteristics which  
 381 then enhance the maximum image pressure  $p_{i,max}$ . It results in a higher peak strength as well as an  
 382 enhancement of the hardening and softening rates which infer additional brittleness to the material  
 383 and a higher susceptibility to strain localization.

384 The Nor-Sand model considers the tangent elastic properties which are those of an unloading-  
 385 reloading cycle. It is widely accepted that the shear modulus  $G$  increases with pressure (Eq. 22).

$$G = A \left( \frac{p'}{p_{ref}} \right)^n \quad (22)$$

386 Alonso et al. (2010) suggested a similar expression in which the enhancement of the elastic  
 387 properties is solely captured by the enhancement of the effective stress. The bulk modulus  $K$  may  
 388 then be deduced from the shear modulus (Eq. 23). The Poisson ratio is assumed to be constant.

$$K = \frac{2(1 + \nu)}{3(1 - 2\nu)} \cdot G \quad (23)$$

389 where  $G$  is the shear modulus,  $A$  is the shear modulus constant,  $n$  the shear modulus exponent,  
 390  $p_{ref}$  the unit reference pressure,  $K$  the bulk modulus and  $\nu$  the Poisson ratio.

### 391 **Simulating triaxial compression tests**

392 The calibration of the model parameters is obtained from laboratory tests with the exception  
 393 of the hardening modulus  $H$  and the dilatancy parameter of the yield function  $N_f$ . The values of  
 394 the model parameter are summarized in Table 2. The elastic parameters ( $A$ ,  $n$ ,  $p_{ref}$ ) have been  
 395 calibrated on an unloading and reloading cycle and the Poisson ratio  $\nu$  was taken as a constant.  
 396 The critical state effective stress ratio  $M$  and the dilatancy coefficient for the potential function  $N_p$   
 397 were obtained from the stress-dilatancy curves. The dilatancy coefficient for the yield surface  $N_f$

398 was progressively reduced from  $N_f = N_p$  until matching the experimental data. The minimum and  
399 maximum void ratios  $e_{min}$  and  $e_{max}$  were obtained by laboratory testing. The crushing pressure  
400  $Q$  is given in Bolton (1986). The minimum hardening modulus  $H_{min}$  and its coefficient  $\delta_H$  were  
401 obtained empirically. The saturated dilatancy coefficient  $X_{sat}$ , its maximum enhancement  $\Delta X$  and  
402 the shape function coefficient  $\beta_{wet}$  were obtained from the dilatancy analysis. The shape function  
403 parameter  $\beta_{dry}$  was set at 0.5 arbitrarily as no data was available and no simulations will be carried  
404 out in that region of saturation.

405 The triaxial compression tests, presented in Fig. 3, were simulated using a single-element code  
406 and the results are presented in Fig. 10 and 11. The simulations of the dense specimens (Fig. 10a-b  
407 and 11a-b) are in agreement with the experimental data. The hardening phase, the peak strength  
408 and the minimum dilatancy rate are well captured by the model. However, some differences emerge  
409 between the simulations and the experimental data in the softening phase. This is largely because  
410 of strain localization, which is accentuated by the enhancement of the dilatancy characterized, and  
411 cannot be captured by single-element simulations. However, the Nor-Sand model is capable of  
412 capturing the formation of shear bands as it was demonstrated by Andrade (2006).

413 The simulations of the medium-dense specimens (Fig. 10c-d and 11c-d) are in better agreement  
414 with the experimental data due to the absence of strain localization. The hardening phase, the  
415 peak strength and the minimum dilatancy rate were well captured by the model as well as the  
416 softening phase due to the absence of strain localization. The specimens, therefore, underwent a  
417 homogeneous failure which is in accordance with the stress-dilatancy and critical state theories.

418 The simulations of the loose specimens (Fig. 10e-f and 11e-f) are in good agreement with the  
419 experimental data. Both the simulations and the experimental data show small dilatancy rates and,  
420 hence, peak strengths. Furthermore, the stiffness in the hardening phase is reduced. However,  
421 loose specimens have initial void ratios close to the critical state line and, therefore, small errors  
422 in the estimation of the initial void ratio as well as small errors in the modeling of the critical state  
423 line lead to errors in the estimation of the dilatancy rate. The mechanical behavior of loose sand is  
424 sensitive to its initial density. This issue has been pointed out by Jefferies and Been (2006) who

425 highlighted the importance of obtaining accurate initial void ratios. This sensitivity is increased at  
426 low pressures where dilatancy is more significant.

427 The overall results of the simulations are very consistent with the experimental data and this  
428 over a wide range of densities and for three different pressures. Unlike classical elastic-plastic  
429 models, the presented model is able to capture the correct peak strength and dilatancy rates of  
430 partially saturated sand and this with only four additional parameters.

### 431 **Simulating wetting-collapses**

432 The collapse of soil upon wetting is a major concern in terms of understanding and modeling  
433 of unsaturated soil. Leonards (1962) suggested that the collapse was due to a rearrangement of  
434 the grains resulting in a smaller packing and, therefore, a loss of dilatancy characteristics. Alonso  
435 et al. (1990) succeeded in modeling the wetting-collapse by introducing the loading-collapse (LC)  
436 curve which assumes that the on-set of collapse was a yielding point. However, as Russell and  
437 Khalili (2006) and Masin and Khalili (2008) demonstrated, the inclusion the loading-collapse is  
438 only a necessity for models which consider the peak state as a yielding point.

439 Fig. 12 shows a triaxial compression tests in which wetting was undertaken at an axial strain  
440 of 4% (point B). As wetting took place, the dilatancy characteristics and the mean effective stress,  
441 albeit more limited, decreased which caused a decrease of the maximum image pressure and,  
442 hence, the peak state. From point B to C, the maximum image pressure was larger than the image  
443 pressure and the model predicted some swelling. The hardening rule (Eq. 20) was positive. From  
444 point C to D, the maximum image pressure was smaller than the image pressure and the model  
445 predicted a collapse. The hardening rule (Eq. 20) was negative. Fig. 13 illustrates both behaviors.  
446 The continuous line corresponds to the yield surface defined by the current image pressure. The  
447 dashed line corresponds to the peak state yield surface defined by the maximum image pressure.

448 The ability of the model to capture both the enhancement of the peak strength and the wetting  
449 behaviors is not a coincidence. The size of the maximum yield surface is controlled by the dilatancy  
450 characteristics. When the soil is wetted, the loss of dilatancy caused the maximum yield surface  
451 to shrink. Therefore, the predicted peak strength is lower. If the maximum yield surface shrinks

452 sufficiently to be smaller than the current yield surface, a collapse will occur. The large collapse  
453 shown in Fig. 12 is due to the large loss of dilatancy characteristics of Chiba sand. Sands with  
454 smaller dilatancy characteristics would result in smaller collapses.

## 455 **CONCLUSIONS**

456 The investigation of the stress-dilatancy relationship of an unsaturated silica sand showed that  
457 the stress-dilatancy theory was still valid. The increase in peak strength was found to be solely a  
458 consequence of an increase of the dilatancy characteristics. These increases are consistent with a  
459 modification of the soil fabric. The formation of menisci at inter-particle contact which change the  
460 way packets of grains override one another. The modification of the dilatancy characteristics also  
461 explains the changes in the hardening and softening rates and, hence, the higher susceptibility of  
462 partially saturated dense sand to undergo strain localization (Higo et al. 2011).

463 The use of state indexes as proxies for dilatancy were also found to be valid. However, the  
464 modification of the soil fabric by partial saturation lead to an enhancement of the dilatancy coef-  
465 ficients. This is consistent with observation made for saturated sands. However, it can be argued,  
466 from a micro-mechanical point of view, that the conversion of a state index to a dilatancy rate  
467 cannot be captured by a scalar (*e.g.* Li and Dafalias 2012) and additional investigations should be  
468 undertaken.

469 The validity of the stress-dilatancy rule for unsaturated sand and the ability to predict the peak  
470 state offers unprecedented ease in modeling the mechanical behavior of unsaturated sand. This was  
471 demonstrated with the Nor-Sand model (Jefferies 1993; Borja and Andrade 2006) for which only  
472 four additional parameters were required to capture the increase in shear strength and dilatancy  
473 rates as well as the swelling and collapse by wetting. The proposed modification to the Nor-Sand  
474 model is not unlike the one proposed by Alonso et al. (1990) for the Cam-Clay model but is applied  
475 to the maximum image pressure instead of the preconsolidation pressure and is included the density  
476 as a model variable.

## 477 **ACKNOWLEDGEMENT**

478 The authors would like to thank Dr Takashi Sakanoue from Tokyo Gas, Japan, for his technical

479 and financial support. This project has received funding from the European Unions Seventh Frame-  
480 work Program for research, technological development and demonstration under grant agreement  
481 no PIAP-GA-2012-324522 and from the Swiss National Science Foundation under grant agree-  
482 ment P1SKP2 158621.

## 483 **APPENDIX A - TRIAXIAL COMPRESSION TEST PROGRAM**

484 The specimens for the triaxial tests were prepared to achieve a specific density and water con-  
485 tent. The specimens were then prepared by wet tamping and shaped into 100 mm x 50 mm cylin-  
486 ders. The tamping protocol was strictly followed for each specimen in order to obtain repeatable  
487 test. The specimens were consolidated to a specific net pressure. The pressure were chosen to be  
488 low in order to favor the dilative behavior of Chiba sand.

489 The constant-water-content tests were carried out as 'undrained' in the sense the mass of water  
490 was conserved throughout the test in a similar way Russell (2004) did for Kurnell sand. The  
491 volume change was monitored with the cell water and care was taken to avoid any entrapment  
492 of air in the cell volume which would lead to errors in the assessment of the volumetric strain  
493 increments used to compute the dilatancy rates and the degrees of saturation. The pressure was  
494 kept constant during the entire shearing process. The peak state, which is of concern, was reached  
495 in less than 15 minutes for the longest test and around 3 minutes for the shortest. Therefore,  
496 secondary deformation of the cell casing can be neglected. Furthermore, the tests carried out at  
497 0.1%/min and 5.0%/min were exact duplicates and showed consistent changes in volume. Tables  
498 3 and 4 give the initial state after consolidation.

499 The matric suctions were estimated from the degree of saturation using the water retention  
500 curves (Fig. 1b). These curves were obtained on the drying path which is consistent with dilative  
501 sand. The influence of the hysteresis on the effective stress is expected to be significantly lower  
502 than the influence of strain localization on the critical state strength. The suction of sand is very  
503 low and the suction-induced effective stress less than 10 kPa.

## 504 **NOTATION**

505 *The following symbols are used in this paper:*



506  $a$  = micro-structure exponent;  
507  $A$  = shear modulus constant;  
508  $D$  = dilatancy rate;  
509  $D_{min}$  = minimum dilatancy rate;  
510  $D_{1,max}$  = maximum axial dilatancy rate;  
511  $d$  = grain size;  
512  $e$  = void ratio;  
513  $e_{cs}$  = critical state void ratio;  
514  $e_{max}$  = maximum state void ratio;  
515  $e_{min}$  = minimum void ratio;  
516  $f$  = shape function;  
517  $F$  = yield function;  
518  $P$  = potential function;  
519  $G$  = shear modulus;  
520  $H$  = hardening modulus;  
521  $H_{min}$  = minimum hardening modulus;  
522  $I_C$  = relative pressure index;  
523  $I_D$  = relative density index;  
524  $I_R$  = relative dilatancy index;  
525  $K$  = bulk modulus;  
526  $M$  = critical state stress ratio;  
527  $m_w$  = van Genuchten model parameter;  
528  $N$  = dilatancy parameter;  
529  $N_f$  = dilatancy parameter for yield function;  
530  $N_p$  = dilatancy parameter for potential function;  
531  $n$  = shear modulus exponent;  
532  $n_w$  = van Genuchten model parameter;

533  $p_a$  = pore air pressure;

534  $p_w$  = pore water pressure;

535  $p'$  = mean effective stress;

536  $p'_{cs}$  = critical state mean effective stress;

537  $p'_{max}$  = maximum mean effective stress;

538  $p'_i$  = image pressure of yield function;

539  $p'_{i,p}$  = image pressure of potential function;

540  $p'_{i,max}$  = maximum image pressure;

541  $p'_{ref}$  = reference unit pressure;

542  $p^{net}$  = mean net stress;

543  $p^{tot}$  = mean total pressure;

544  $q$  = deviatoric stress;

545  $q_{cs}$  = critical state deviatoric stress;

546  $Q$  = crushing pressure;

547  $s$  = matric suction;

548  $s_e$  = air entry matric suction;

549  $S_{res}$  = residual degree of saturation;

550  $S_w$  = degree of saturation;

551  $S'_w$  = effective degree of saturation;

552  $S_w^{max}$  = maximum strength degree of saturation;

553  $\alpha$  = dilatancy coefficient;

554  $\alpha_w$  = van Genuchten model parameter;

555  $\beta$  = shape function coefficient;

556  $\delta_H$  = hardening modulus coefficient;

557  $\Delta X$  = dilatancy coefficient enhancement;

558  $\varepsilon_1$  = axial strain;

559  $\varepsilon_d$  = deviatoric strain;

560  $\varepsilon_d^p$  = plastic deviatoric strain;  
561  $\varepsilon_v$  = volumetric strain;  
562  $\varepsilon_v^p$  = plastic volumetric strain;  
563  $\eta'$  = effective stress ratio;  
564  $\eta'_{max}$  = maximum effective stress ratio;  
565  $X$  = dilatancy coefficient;  
566  $X_{sat}$  = saturated dilatancy coefficient;  
567  $\chi$  = Bishop's coupling parameter;  
568  $\psi$  = state parameter;  
569  $\nu$  = Poisson ratio;

570

## 571 REFERENCES

- 572 Aitchison, G. D. (1960). "Relationships of moisture stress and effective stress functions in unsatu-  
573 rated soils." *Conf. Pore Pressures and Suction in Soils*, London, Butterworths.
- 574 Alonso, E., Gens, A., and Josa, A. (1990). "A constitutive model for partially saturated soils."  
575 *Géotechnique*, 40(3), 405–430.
- 576 Alonso, E., Pereira, J.-M., Vaunat, J., and Olivella, S. (2010). "A microstructurally based effective  
577 stress for unsaturated soils." *Géotechnique*, 60(12), 913–925.
- 578 Andrade, J. (2006). "Meso-scale finite element simulation of deformation banding in fluid-saturated  
579 sands." Ph.D. thesis, Stanford University, Stanford University.
- 580 Bardet, J. P. (1986). "Bounding Surface Plasticity Model for Sand." *Journal of Engineering Me-*  
581 *chanics*, 112(11), 1198–1217.
- 582 Been, K. and Jefferies, M. G. (1985). "A state parameter for sands." *Géotechnique*, 35(2), 99–112.
- 583 Bishop, A. (1959). "The principles of effective stress." *Tecnisk Ukeblad*, 8, 859–863.
- 584 Bishop, A. and Blight, G. (1963). "Some Aspects of Effective Stress in Saturated and Partly Satu-  
585 rated Soils." *Géotechnique*, 13(3), 177–197.
- 586 Bolton, M. (1986). "The strength and dilatancy of sands." *Géotechnique*, 36(1), 65–78.

587 Bolzon, G., Schrefler, B. A., and Zienkiewicz, O. C. (1996). "Elastoplastic soil constitutive laws  
588 generalized to partially saturated states." *Géotechnique*, 46(2), 279–289.

589 Borja, R. I. and Andrade, J. E. (2006). "Critical state plasticity. Part VI: Meso-scale finite element  
590 simulation of strain localization in discrete granular materials." *Computer Methods in Applied  
591 Mechanics and Engineering*, 195(37-40), 5115–5140.

592 Chiu, C. F. and Ng, C. (2003). "A state-dependent elasto-plastic model for saturated and unsatu-  
593 rated soils." *Géotechnique*, 53(9), 809–829.

594 Coleman, J. D. (1962). "Stress-strain relations for partly saturated soil." *Géotechnique*, 12(4), 348–  
595 350.

596 Cui, Y. and Delage, P. (1996). "Yielding and plastic behaviour of an unsaturated compacted silt."  
597 *Géotechnique*, 46(2), 291–311.

598 Dafalias, Y. F. and Popov, E. P. (1975). "A model of nonlinearly hardening materials for complex  
599 loading." *Acta Mechanica*, 21(3), 173–192.

600 Desrues, J., Chambon, R., Mokni, M., and Mazerolle, F. (1996). "Void ratio evolution inside shear  
601 bands in triaxial sand specimens studied by computed tomography." *Géotechnique*, 46(3), 529–  
602 546.

603 Donald, I. B. (1956). "Shear Strength Measurements." *2nd Australian-New Zealand Conference  
604 on Soil Mechanics and Foundation Engineering*, Christchurch, The New Zealand Institution of  
605 Engineers, 200–204.

606 D'Onza, F., Gallipoli, D., Wheeler, S., Casini, F., Vaunat, J., Khalili, N., Laloui, L., Mancuso, C.,  
607 Masin, D., Nuth, M., Pereira, J. M., and Vassallo, R. (2011). "Benchmark of constitutive models  
608 for unsaturated soils." *Géotechnique*, 61(4), 283–302.

609 Drucker, D., Gibson, R., and Henkel, D. (1957). "Soil mechanics and work-hardening theories of  
610 plasticity." *Journal of Soil Mechanics and Foundation Engineering* 1, 122, 338–346.

611 Fern, J., Robert, D., Sakanoue, T., and Soga, K. (2015). "Shear Strength and Dilatancy of Un-  
612 saturated Silica Sand in Triaxial Compression Tests." *Computer Methods and Recent Advances  
613 in Geomechanics*, F. Oka, A. Murakami, R. Uzuoka, and S. Kimoto, eds., London, Taylor &

614 Francis, 535–540.

615 Fredlund, D. G., Morgenstern, N. R., and Widger, R. A. (1978). “The shear strength of unsaturated  
616 soils.” *Canadian Geotechnical Journal*, 15(3), 313–321.

617 Geiser, F. (1999). “Comportement mécanique d’un limon non saturé : étude expérimentale et  
618 modélisation constitutive.” Ph.D. thesis, Ecole Polytechnique fédérale de Lausanne, Ecole Poly-  
619 technique fédérale de Lausanne.

620 Hashiguchi, K. and Chen, Z. P. (1998). “Elastoplastic Constitutive Equation of Soils With the  
621 Subloading Surface.” *International Journal*, 22(June 1996), 197–227.

622 Higo, Y., Oka, F., Kimoto, S., Sanagawa, T., and Matsushima, Y. (2011). “Study of Strain Lo-  
623 calization and Microstructural Changes in Partially Saturated Sand During Triaxial Tests Using  
624 Microfocus X-Ray CT.” *Soils and foundations*, 51(1), 95–111.

625 Jefferies, M. (1993). “Nor-Sand : a simple critical state model for sand.” *Géotechnique*, 43(1),  
626 91–103.

627 Jefferies, M. and Been, K. (2006). *Soil Liquefaction A Critical State Approach*. Taylor & Francis,  
628 London.

629 Jefferies, M. and Shuttle, D. (2002). “Dilatancy in general Cambridge-type models.” *Géotechnique*,  
630 52(9), 625–638.

631 Jefferies, M. and Shuttle, D. (2011). “On the operating critical friction ratio in general stress states.”  
632 *Géotechnique*, 61(8), 709–713.

633 Jennings, J. and Burland, J. (1962). “Limitations to the Use of Effective Stresses in Partly Saturated  
634 Soils.” *Géotechnique*, 12(2), 125–144.

635 Khalili, N., Geiser, F., and Blight, G. (2004). “Effective Stress in Unsaturated Soils: Review with  
636 New Evidence.” *International Journal of Geomechanics*, 4(2), 115–126.

637 Khalili, N. and Khabbaz, M. H. (1998). “A unique relationship for  $\chi$  for the determination of the  
638 shear strength of unsaturated soils.” *Géotechnique*, 48(5), 681–687.

639 Lam, W. and Tatsuoka, F. (1988). “Effects of initial anisotropic fabric and .SIGMA.2 on strength  
640 and deformation characteristics of sand..” *Soils and Foundations*, 28(1), 89–106.

641 Leonards, G. (1962). "Discussion of Jennings and Burland 'Limitations to the use of effective  
642 stress in partly saturated soils'." *Géotechnique*, 12(4), 354–355.

643 Li, X. and Dafalias, Y. (2012). "Anisotropic Critical State Theory: Role of Fabric." *Journal of*  
644 *Engineering Mechanics*, 138(3), 263–275.

645 Likos, W. J., Wayllace, A., Godt, J., and Lu, N. (2010). "Modified direct shear apparatus for  
646 unsaturated sands at low suction and stress." *Geotechnical Testing Journal*, 33(4), 1–13.

647 Loret, B. and Khalili, N. (2000). "A three-phase model for unsaturated soils." *International Journal*  
648 *for Numerical and Analytical Methods in Geomechanics*, 24(March 1999), 893–927.

649 Lu, N. and Likos, W. J. (2004). *Unsaturated Soil Mechanics*. John Wiley & Sons, Hoboken.

650 Lu, N. and Likos, W. J. (2006). "Suction Stress Characteristic Curve for Unsaturated Soil." *Journal*  
651 *of Geotechnical and Geoenvironmental Engineering*, 132(2), 131–142.

652 Maatouk, A., Leroueil, S., and La Rochelle, P. (1995). "Yielding and critical state of a collapsible  
653 unsaturated silty soil." *Géotechnique*, 45(3), 465–477.

654 Masin, D. and Khalili, N. (2008). "A hypoplastic model for mechanical response of unsaturated  
655 soils." *International Journal for Numerical and Analytical Methods in Geomechanics*, 32(15),  
656 1903–1926.

657 Mitchell, J. and Soga, K. (2005). *Fundamentals of Soil Behavior*. John Wiley & Sons, Hoboken,  
658 3rd edition.

659 Ng, C. and Menzies, B. (2007). *Advanced unsaturated soil mechanics and engineering*. Taylor &  
660 Francis, New York.

661 Nova, R. (1982). "A constitutive model for soil under monotonic and cyclic loading." *Soil me-*  
662 *chanics - transient and cyclic loading*, G. N. Pande and C. Zienkiewicz, eds., Chichester, Wiley,  
663 343–373.

664 Nuth, M. (2009). "Constitutive Modelling of Unsaturated Soils with Hydro-Geomechanical Cou-  
665 plings." *Report no.*, Ecole Polytechnique Fédérale de Lausanne.

666 Oda, M. (1972). "The Mechanism of Fabric Changes during Compressional deformation of sand."  
667 *Soils and Foundations*, 12(2), 1–18.

668 Rampino, C., Mancuso, C., and Vinale, F. (2000). “Experimental behaviour and modelling of an  
669 unsaturated compacted soil.” *Canadian Geotechnical Journal*, 37(4), 748–763.

670 Robert, D. (2010). “Soil-Pipeline Interaction in Unsaturated Soils.” Ph.d. dissertation, University  
671 of Cambridge, University of Cambridge.

672 Roscoe, K. H. (1970). “The Influence of Strains in Soil Mechanics.” *Géotechnique*, 20(2), 129–  
673 170.

674 Roscoe, K. H. and Burland, J. B. (1968). “On the generalised stress-strain behaviour of ‘wet’ clay.”  
675 *Engineering plasticity*, J. Heyman and F. Leckie, eds., Cambridge, Cambridge University Press,  
676 535–609.

677 Roscoe, K. H. and Schofield, A. (1963). “Mechanical behaviour of an idealised wet clay.” *2nd*  
678 *European Conference on Soil Mechanics and Foundation Engineering*, Wiesbaden, 47–54.

679 Roscoe, K. H., Schofield, A., and Wroth, C. P. (1958). “On The Yielding of Soils.” *Géotechnique*,  
680 8(1), 22–53.

681 Russell, A. (2004). “Cavity Expansion in Unsaturated Soils.” Ph.D. thesis, University of New  
682 South Wales, University of New South Wales.

683 Russell, A. and Khalili, N. (2006). “A unified bounding surface plasticity model for unsaturated  
684 soils.” *International Journal for Numerical and Analytical Methods in Geomechanics*, 30(3),  
685 181–212.

686 Schnellmann, R., Rahardjo, H., and Schneider, H. R. (2013). “Unsaturated shear strength of a silty  
687 sand.” *Engineering Geology*, 162, 88–96.

688 Scholtès, L., Hicher, P.-Y., Nicot, F., Chareyre, B., and Darve, F. (2009). “On the capillary stress  
689 tensor in wet granular materials.” *International Journal for Numerical and Analytical Methods*  
690 *in Geomechanics*, 33(10), 1289–1313.

691 Stroud, M. (1971). “The behaviour of sand at low stress levels in the simple-shear apparatus.”  
692 Ph.D. thesis, University of Cambridge, University of Cambridge.

693 Tatsuoka, F. (1987). “Discussion: The strength and dilatancy of sands.” *Géotechnique*, 37(2), 219–  
694 226.

- 695 Taylor, D. (1948). *Fundamentals of soil mechanics*. Wiley, New York.
- 696 Toll, D. (1988). “The behaviour of unsaturated compacted naturally occurring gravel.” Ph.D. thesis,  
697 University of London, University of London.
- 698 Toll, D. (1990). “A framework for unsaturated soil behaviour.” *Géotechnique*, 40(1), 31–44.
- 699 Toll, D. and Ong, B. (2003). “Critical-state parameters for an unsaturated residual sandy clay.”  
700 *Géotechnique*, 53(1), 93–103.
- 701 van Genuchten, M. (1980). “A closed form equation for predicting the hydraulic conductivity of  
702 unsaturated soils.” *Soil Science Society American Journal*, 44, 892–898.
- 703 Vanapalli, S., Fredlund, D. G., Pufahl, D., and Clifton, A. (1996). “Model for the Prediction of  
704 Shear Strength with Respect to Soil Suction.” *Canadian Geotechnical Journal*, 33, 379–392.
- 705 Verdugo, R. and Ishihara, K. (1996). “The Steady State of Sandy Soils.” *Soils and Foundations*,  
706 36(2), 81–91.
- 707 Wheeler, S. J. and Sivakumar, V. (1995). “An elasto-plastic critical state framework for unsaturated  
708 soil.” *Géotechnique*, 45(1), 35–53.



709

**List of Tables**

710        1    van Genuchten (1980) SWRC parameters for Chiba sand . . . . . 31

711        2    Unsaturated Nor-Sand parameters for Chiba sand. . . . . 32

712        3    Initial conditions for long duration triaxial compression tests . . . . . 33

713        4    Initial conditions for short duration triaxial compression tests . . . . . 34

**TABLE 1. van Genuchten (1980) SWRC parameters for Chiba sand**

$e$	$S_{res}$	$\alpha_w$	$n_w$	$m_w$
[-]	[-]	[kPa <sup>-1</sup> ]	[-]	[-]
0.963	20%	0.50	3.0	0.3
0.815	22%	0.38	3.0	0.3
0.699	24%	0.22	3.2	0.3

**TABLE 2. Unsaturated Nor-Sand parameters for Chiba sand.**

Label	Symbol	Value
Shear modulus constant	$A$	2500 kPa
Shear modulus exponent	$n$	0.5
Reference pressure	$p_{ref}$	1 kPa
Critical state effective stress ratio	$M$	1.33
Maximum void ratio	$e_{max}$	0.946
Minimum void ratio	$e_{min}$	0.500
Crushing pressure	$Q$	10 MPa
Dilatancy parameter for yield function	$N_f$	0.35
parameter for potential function	$N_p$	0.3
Minimum hardening modulus	$H_{min}$	160
Hardening modulus coefficient	$\delta_H$	2
Saturated dilatancy coefficient	$X_{sat}$	2.5
Maximum dilatancy coefficient enhancement	$\Delta X$	3.1
Shape function coefficient on dry side	$\beta_{dry}$	0.5
Shape function coefficient on wet side	$\beta_{wet}$	3.0
Degree of saturation at maximum enhancement	$S_w^{max}$	21%

**TABLE 3. Initial conditions for long duration triaxial compression tests**

Group	$w$ [-]	$e_0$ [-]	$S_{w,0}$ [-]	$p_0^{net}$ [kPa]	$d\varepsilon_1$ [%/min]	$I_{D,0}$ [-]	$I_{R,0}$ [-]	$\psi_0$ [-]
Loose	10%	0.842	32%	20	0.1	23%	0.09	-0.01
	10%	0.818	33%	40	0.1	29%	0.47	-0.04
	10%	0.808	34%	80	0.1	30%	0.43	-0.04
	17%	0.845	55%	20	0.1	23%	0.06	-0.01
	17%	0.830	56%	40	0.1	26%	0.28	-0.03
	17%	0.820	56%	80	0.1	28%	0.29	-0.03
Med.-Dense	10%	0.742	37%	20	0.1	46%	1.63	-0.13
	10%	0.738	37%	40	0.1	47%	1.46	-0.12
	10%	0.725	38%	80	0.1	50%	1.34	-0.13
	10%	0.739	37%	40	0.5	46%	1.44	-0.12
	17%	0.745	62%	20	0.1	45%	1.58	-0.12
	17%	0.734	63%	40	0.1	48%	1.52	-0.13
	17%	0.719	64%	80	0.1	51%	1.41	-0.13
	17%	0.734	63%	40	0.5	47%	1.51	-0.13
Dense	27%	0.739	100%	40	0.5	46%	1.44	-0.12
	17%	0.656	41%	20	0.1	65%	2.93	-0.22
	17%	0.659	41%	40	0.1	64%	2.49	-0.20
	17%	0.653	42%	80	0.1	66%	2.14	-0.20
	17%	0.657	70%	20	0.1	65%	2.91	-0.22
	17%	0.648	71%	40	0.1	67%	2.63	-0.22
	17%	0.641	72%	80	0.1	68%	2.28	-0.21

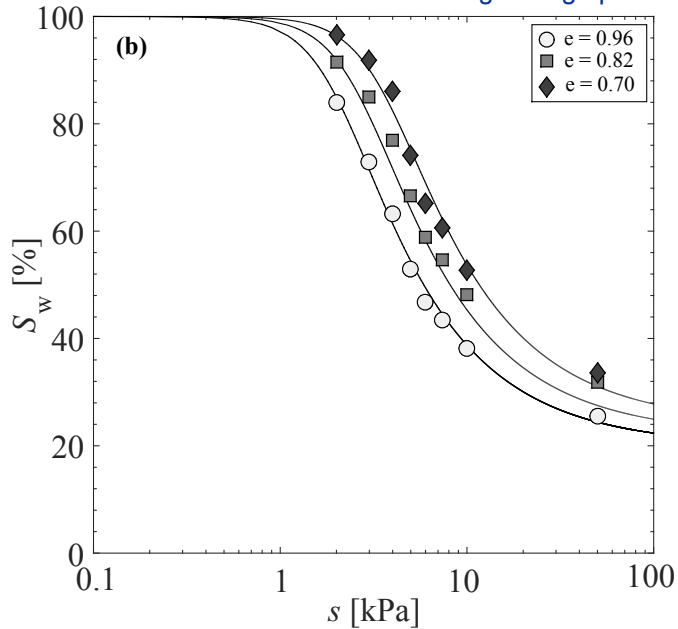
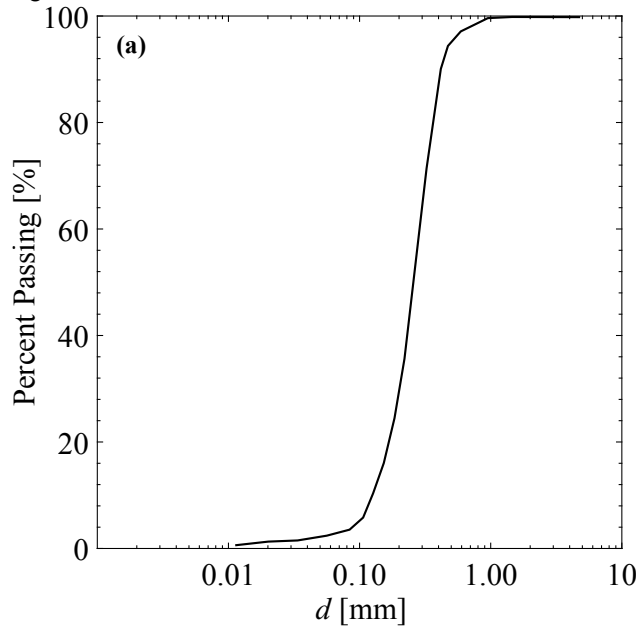
**TABLE 4. Initial conditions for short duration triaxial compression tests**

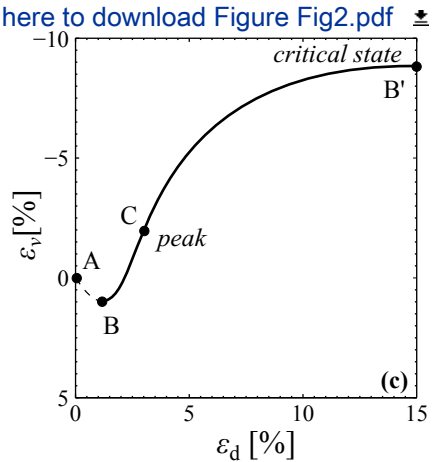
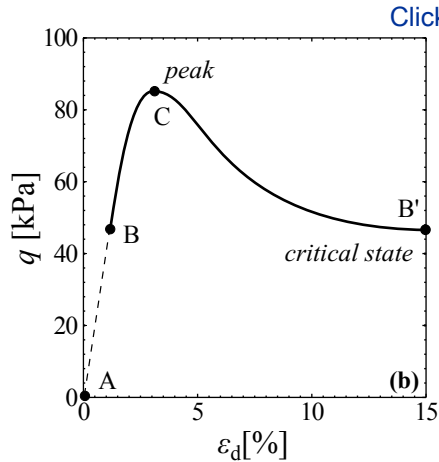
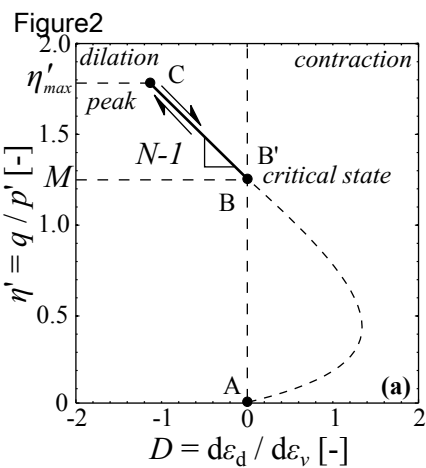
Group	$w$ [-]	$e_0$ [-]	$S_{w,0}$ [-]	$p_0^{net}$ [kPa]	$d\varepsilon_1$ [%/min]	$I_{D,0}$ [-]	$I_{R,0}$ [-]	$\psi_0$ [-]
Loose	10%	0.838	32%	20	5.0	24%	0.38	-0.03
	10%	0.832	33%	40	5.0	26%	0.34	-0.03
	10%	0.823	33%	80	5.0	28%	0.29	-0.03
	17%	0.834	55%	20	5.0	25%	0.53	-0.04
	17%	0.829	56%	40	5.0	26%	0.43	-0.04
	17%	0.816	57%	80	5.0	29%	0.40	-0.04
Med.-Dense	10%	0.741	37%	20	5.0	46%	1.50	-0.12
	10%	0.737	37%	40	5.0	47%	1.37	-0.12
	10%	0.725	38%	80	5.0	50%	1.27	-0.12
	17%	0.742	62%	20	5.0	46%	1.75	-0.13
	17%	0.732	63%	40	5.0	48%	1.60	-0.13
	17%	0.715	65%	80	5.0	52%	1.48	-0.14
Dense	10%	0.655	42%	20	5.0	65%	2.68	-0.21
	10%	0.649	42%	40	5.0	67%	2.46	-0.21
	10%	0.645	42%	80	5.0	67%	2.14	-0.21
	17%	0.656	70%	20	5.0	65%	2.95	-0.22
	17%	0.647	71%	40	5.0	67%	2.66	-0.22
	17%	0.639	72%	80	5.0	69%	2.30	-0.21

## List of Figures

1	(a) Grain-size distribution and (b) water retention curve of Chiba Sand . . . . .	37
2	Schematic description of (a) the stress-dilatancy curve with respect to the development of (b) deviatoric stress and (c) volumetric strains in triaxial compression tests . . . . .	38
3	Stress-dilatancy curves of conventional triaxial compression tests on unsaturated Chiba sand . . . . .	39
4	Relationship between the maximum effective stress ratio and the minimum dilatancy rate . . . . .	40
5	Critical state line based on the relative dilatancy index for (a) saturated Toyoura sand from Verdugo and Ishihara (1996) and (b) saturated and unsaturated Kurnell sand from Russell and Khalili (2006) . . . . .	41
6	Critical state line based on the relative dilatancy index for dry and unsaturated Chiba sand which were carried out as duplicates with axial strain rates of (a) 0.1%/min and (b) 5.0%/min . . . . .	41
7	Relative dilatancy index of triaxial compression tests on unsaturated Chiba sand . . . . .	42
8	(a) Different shape function shapes and (b) the calibration for Chiba sand . . . . .	43
9	Yield and potential surfaces for different values of the dilatancy parameter . . . . .	44
10	Simulation of the constant-water-content triaxial compression tests on partially saturated Chiba sand ( $w = 10\%$ ) . . . . .	45
11	Simulation of the constant-water-content triaxial compression tests on partially saturated sand ( $w = 17\%$ ) . . . . .	46
12	Simulation of a triaxial compression tests of a medium-dense sand ( $e_0 = 0.700$ ) with a wetting path ( $\Delta S_w = +40\%$ ) at $\varepsilon_1 = 4\%$ . . . . .	47
13	Position of the maximum image yield surface defined by the maximum image pressure resulting (a) swelling and (b) a collapse . . . . .	48

Figure 1

[Click here to download Figure Fig1.pdf](#)



[Click here to download Figure Fig2.pdf](#)



Figure 3

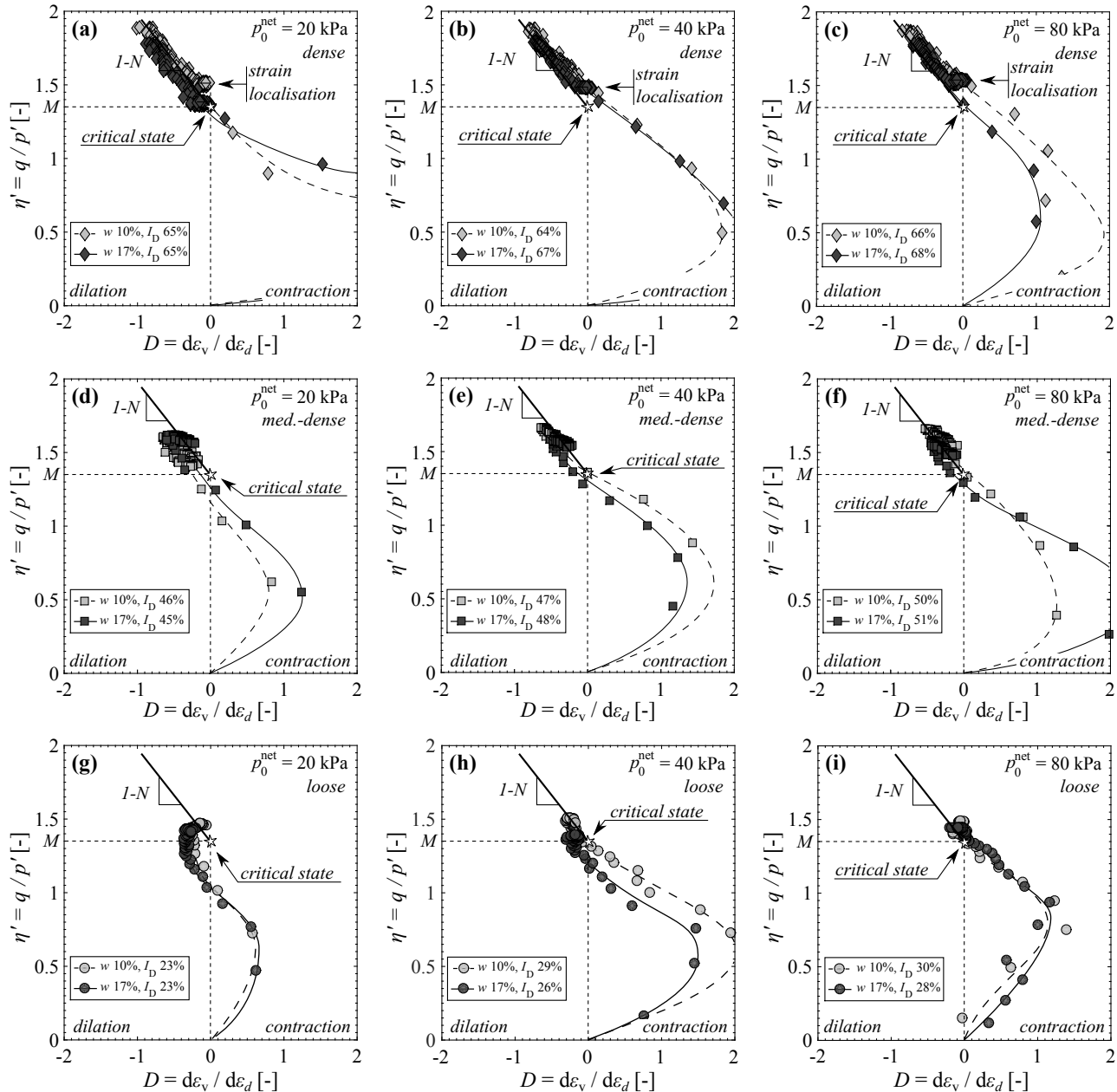


Figure4

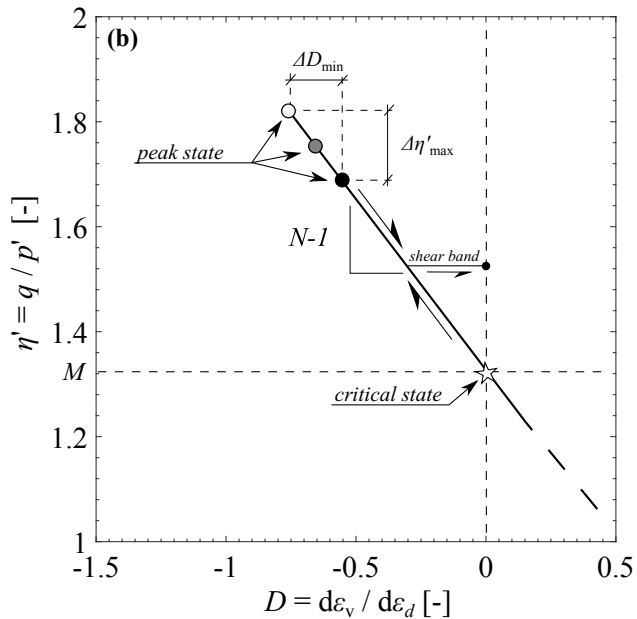
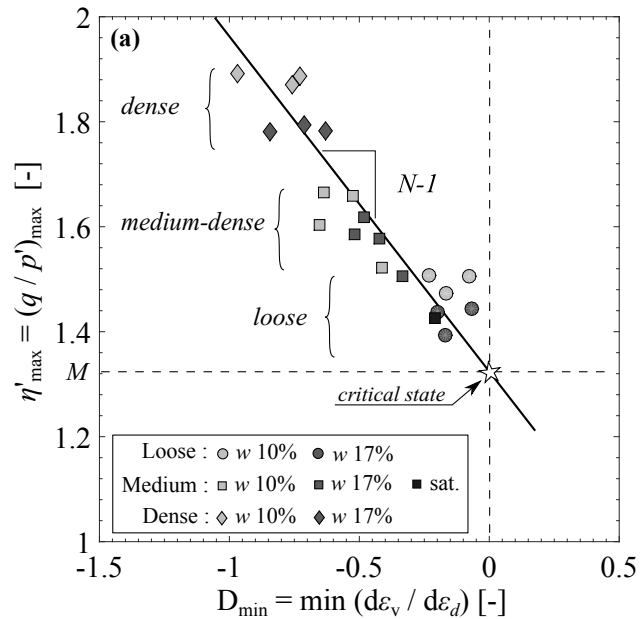
[Click here to download Figure Fig4.pdf](#)

Figure 5

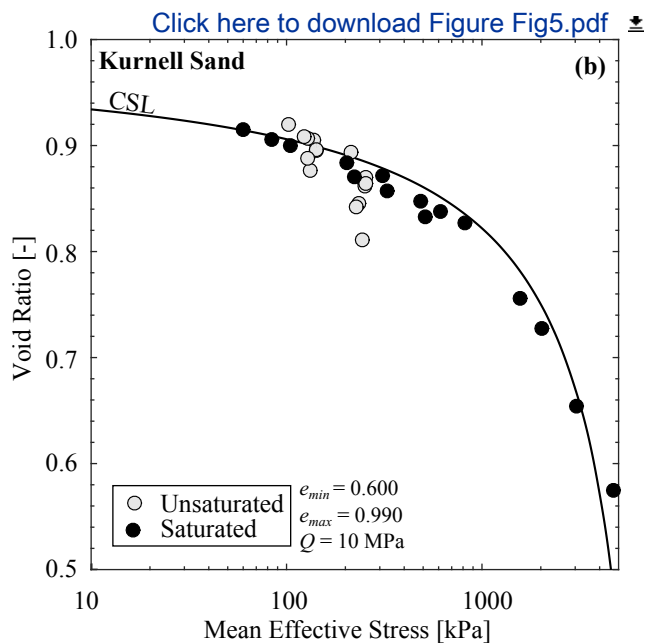
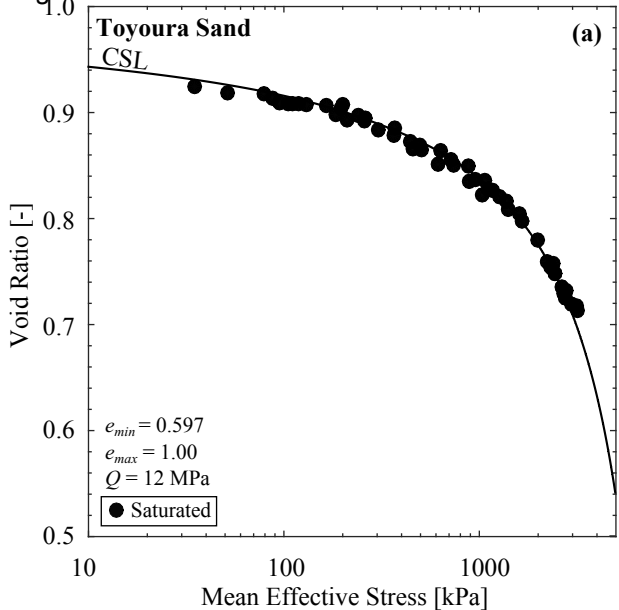


Figure6

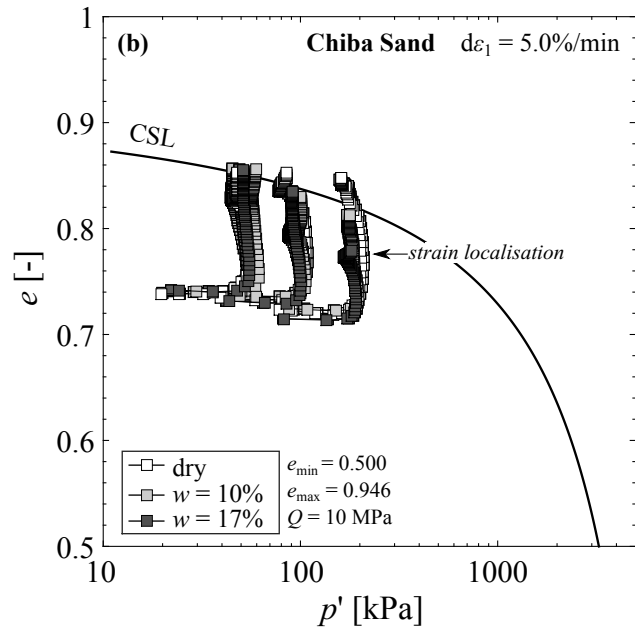
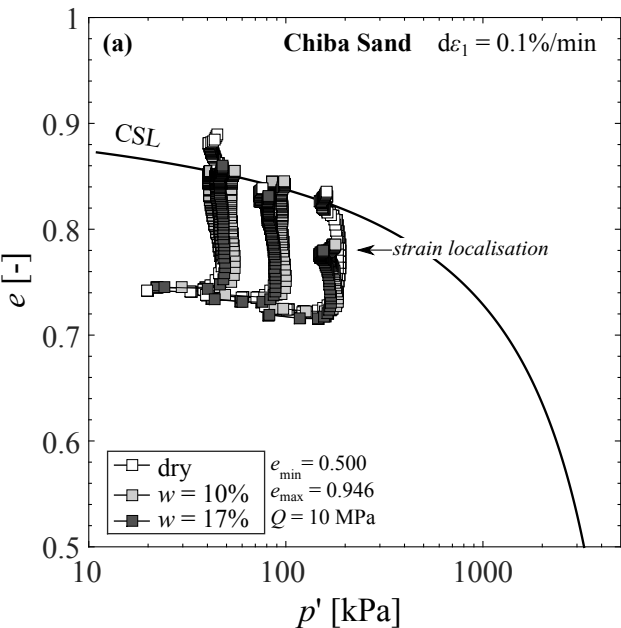
[Click here to download Figure Fig6.pdf](#)

Figure7

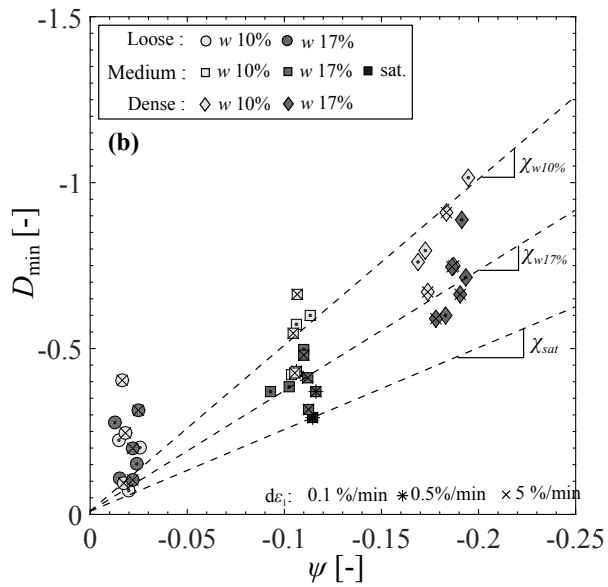
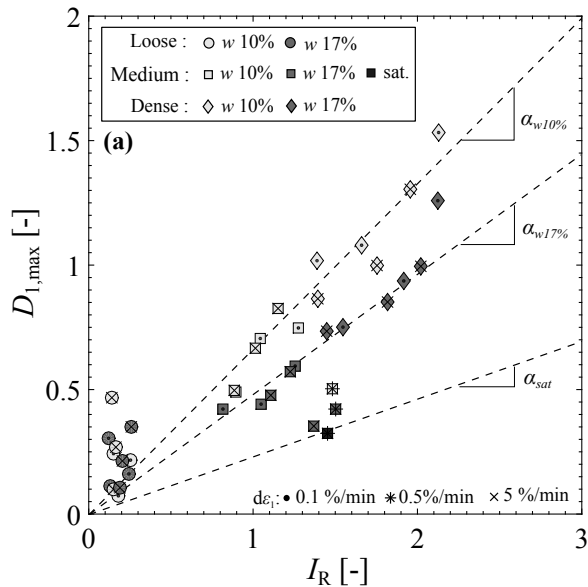
[Click here to download Figure Fig7.pdf](#)

Figure8

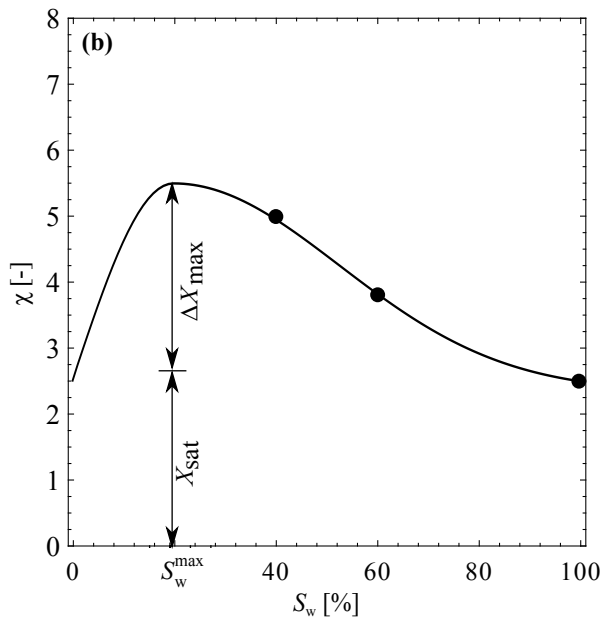
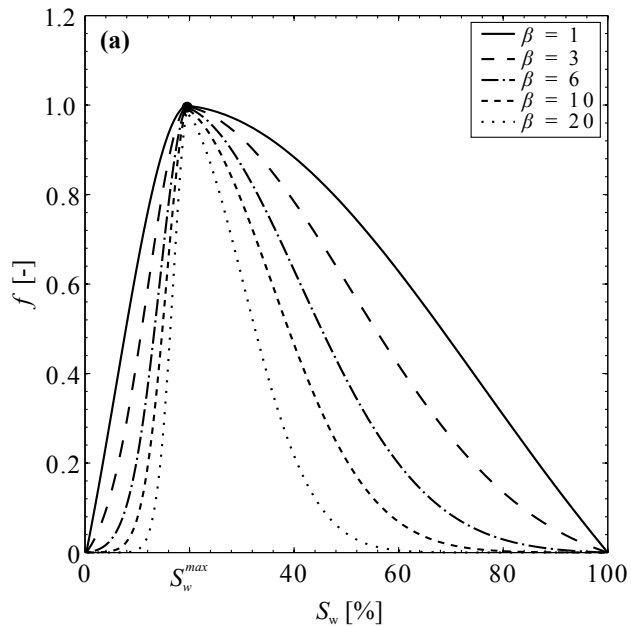
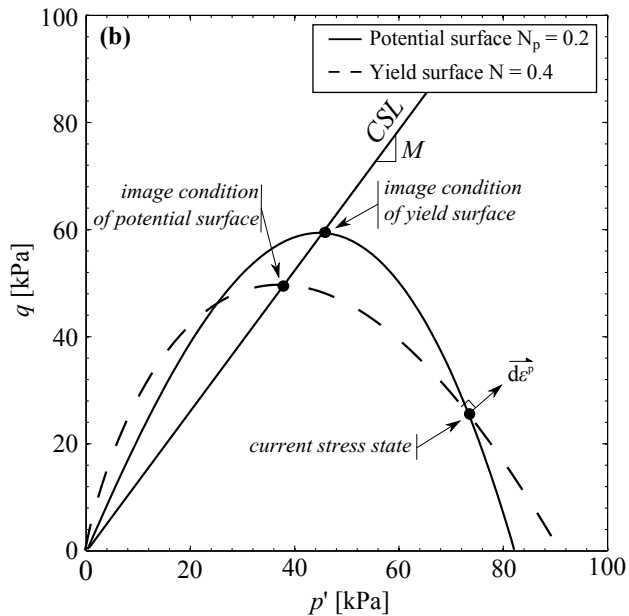
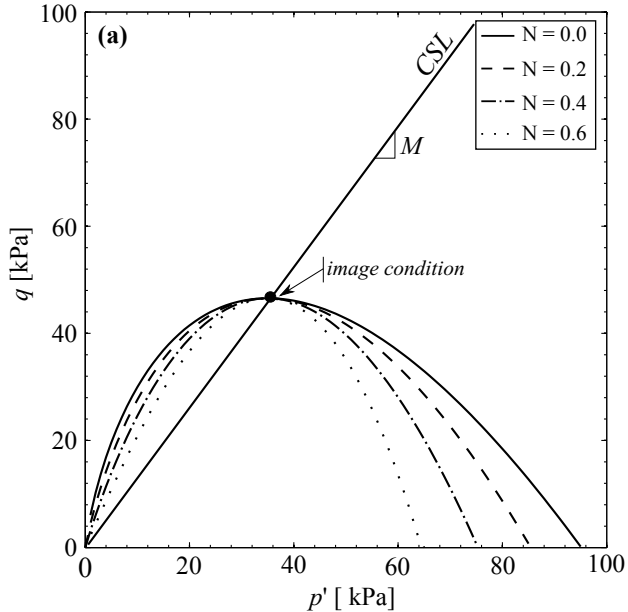
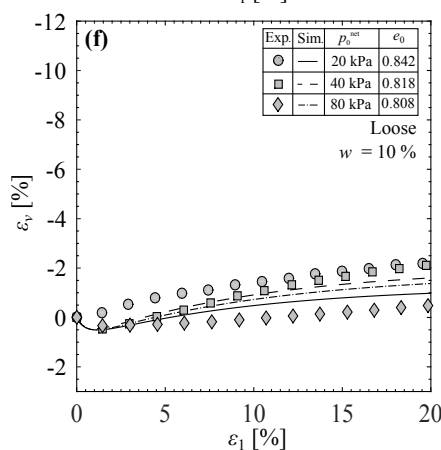
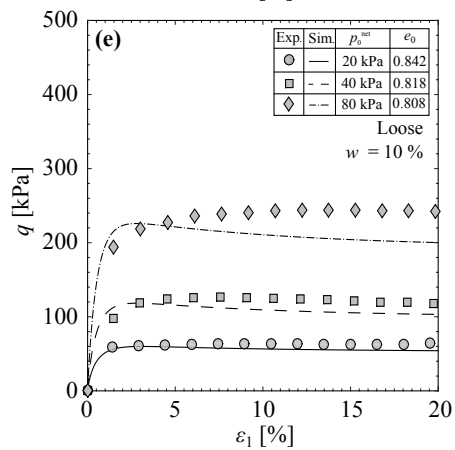
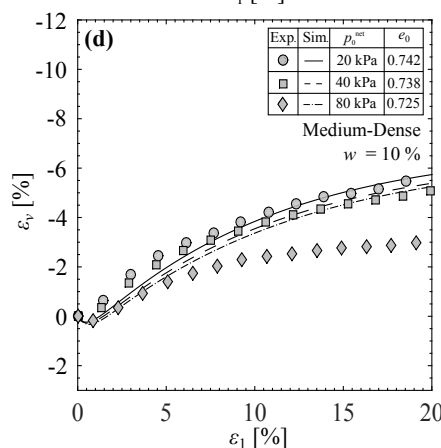
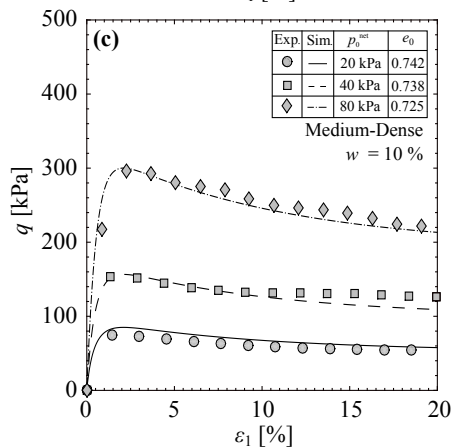
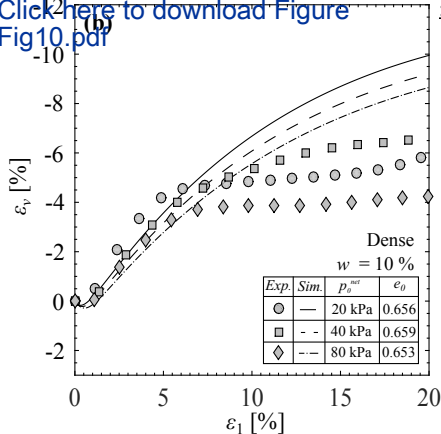
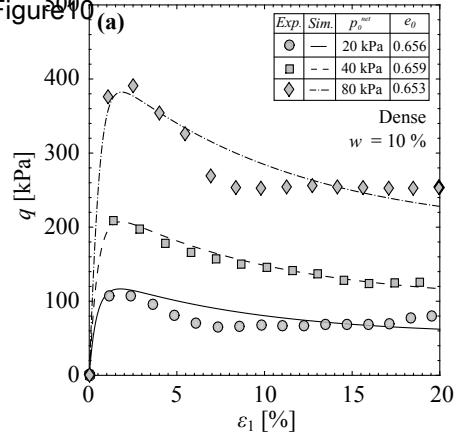
[Click here to download Figure Fig8.pdf](#)

Figure9

[Click here to download Figure Fig9.pdf](#)





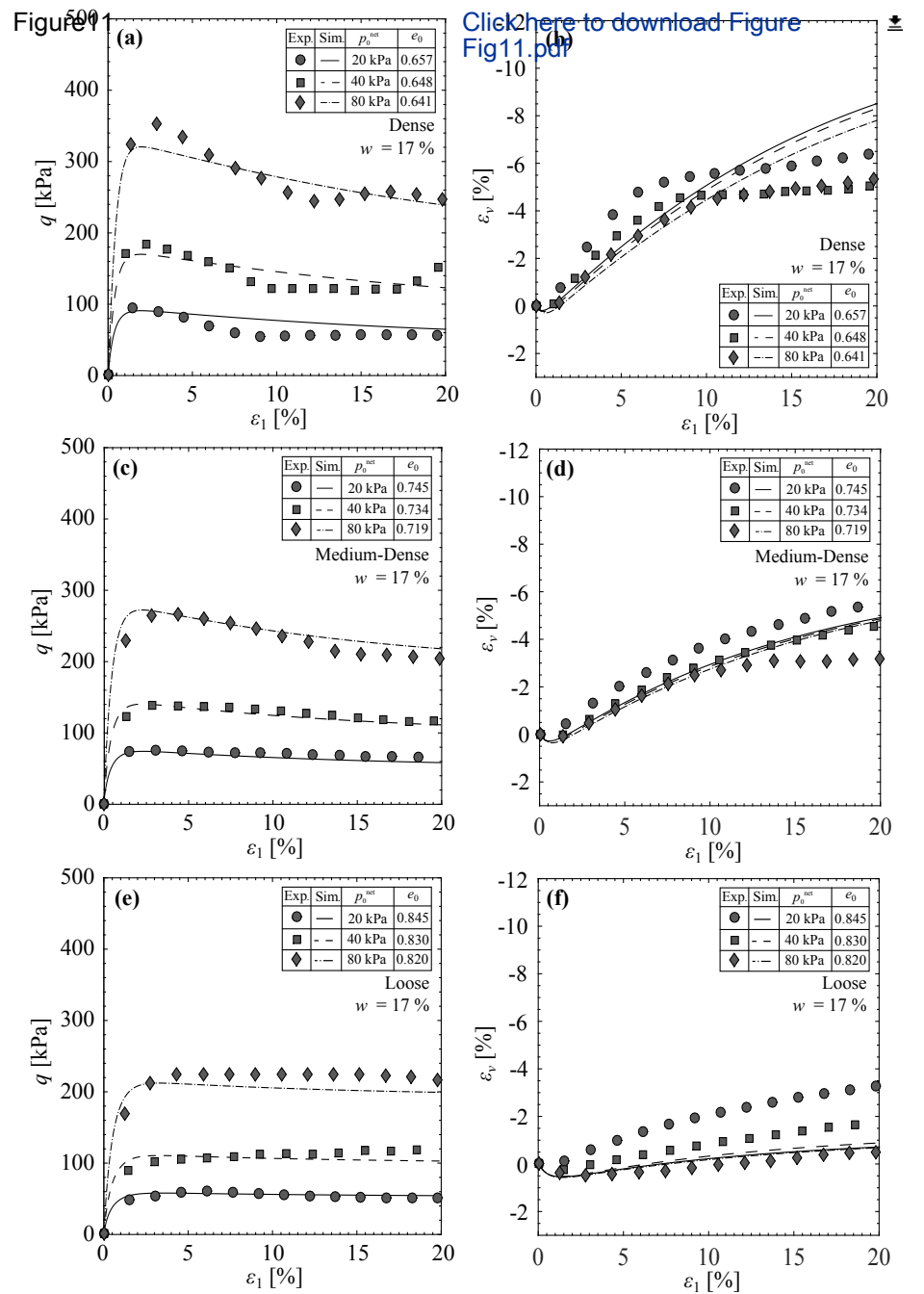


Figure12

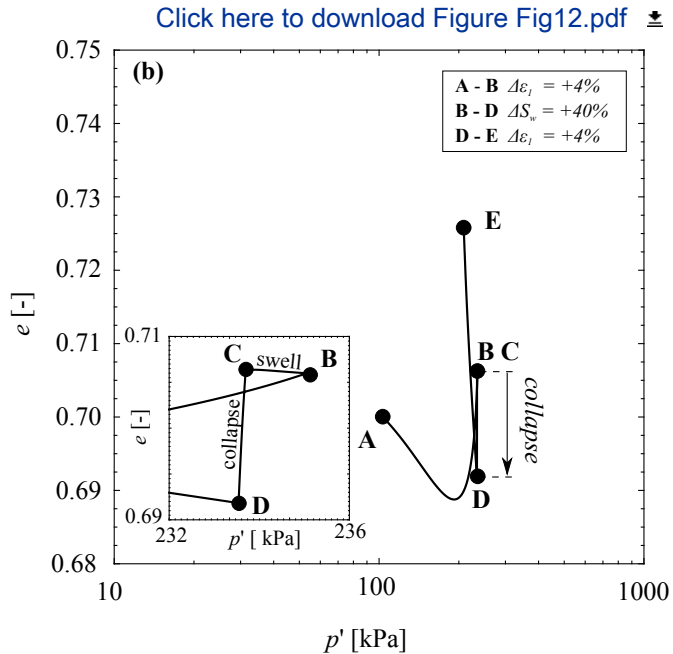
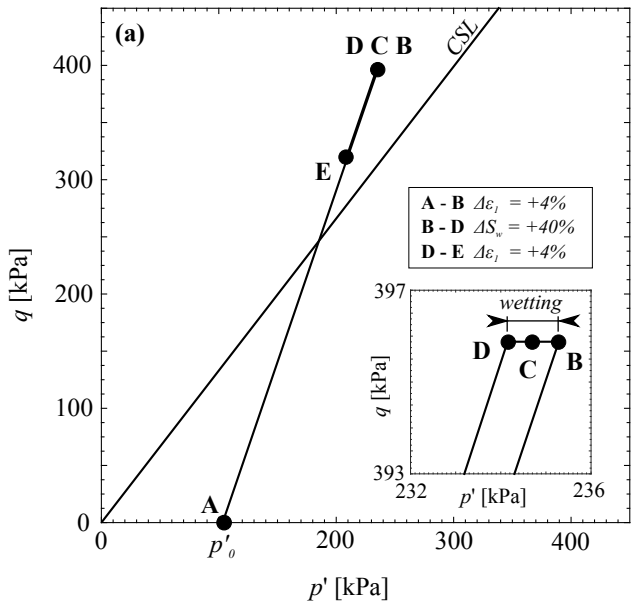


Figure13

[Click here to download Figure Fig13.pdf](#)
